1987

A three-dimensional nodal solution for the frequency dependent neutron diffusion equation

Abdulghani M. Melaibari
Iowa State University

INFORMATION TO USERS

While the most advanced technology has been used to photograph and reproduce this manuscript, the quality of the reproduction is heavily dependent upon the quality of the material submitted. For example:

- Manuscript pages may have indistinct print. In such cases, the best available copy has been filmed.

- Manuscripts may not always be complete. In such cases, a note will indicate that it is not possible to obtain missing pages.

- Copyrighted material may have been removed from the manuscript. In such cases, a note will indicate the deletion.

Oversize materials (e.g., maps, drawings, and charts) are photographed by sectioning the original, beginning at the upper left-hand corner and continuing from left to right in equal sections with small overlaps. Each oversize page is also filmed as one exposure and is available, for an additional charge, as a standard 35mm slide or as a 17"x 23" black and white photographic print.

Most photographs reproduce acceptably on positive microfilm or microfiche but lack the clarity on xerographic copies made from the microfilm. For an additional charge, 35mm slides of 6"x 9" black and white photographic prints are available for any photographs or illustrations that cannot be reproduced satisfactorily by xerography.

Order Number 8721909

A three-dimensional nodal solution for the frequency dependent neutron diffusion equation

Melaibari, Abdulghani M., Ph.D.

Iowa State University, 1987

U·M·I
300 N. Zeeb Rd.
Ann Arbor, MI 48106

PLEASE NOTE:

In all cases this material has been filmed in the best possible way from the available copy. Problems encountered with this document have been identified here with a check mark __✓__.

1. Glossy photographs or pages _____
2. Colored illustrations, paper or print _____
3. Photographs with dark background _____
4. Illustrations are poor copy _____
5. Pages with black marks, not original copy _____
6. Print shows through as there is text on both sides of page _____
7. Indistinct, broken or small print on several pages ✓
8. Print exceeds margin requirements _____
9. Tightly bound copy with print lost in spine _____
10. Computer printout pages with indistinct print _____
11. Page(s) _____ lacking when material received, and not available from school or author.
12. Page(s) _____ seem to be missing in numbering only as text follows.
13. Two pages numbered _____. Text follows.
14. Curling and wrinkled pages _____
15. Dissertation contains pages with print at a slant, filmed as received _____
16. Other _____

_____

_____

A three-dimensional nodal solution for the frequency dependent neutron diffusion equation

by

Abdulghani M. Melaibari

A Dissertation Submitted to the
Graduate Faculty in Partial Fulfillment of the
Requirements for the Degree of
DOCTOR OF PHILOSOPHY

Major: Nuclear Engineering

Approved:

Signature was redacted for privacy.
In Charge of Major Work

Signature was redacted for privacy.
For the Major Department

Signature was redacted for privacy.
For the Graduate College

Iowa State University
Ames, Iowa

1987

TABLE OF CONTENTS

		PAGE
I.	INTRODUCTION	1
II.	LITERATURE REVIEW	3
III.	DEVELOPING THE EQUATIONS	14
IV.	THE REACTOR MODEL	20
V.	THE ANALYTICAL SOLUTION	23
	A. Solution Development	23
	B. Modifying the Solution	28
	1. Applying the Poisson's summation formula	30
	2. Applying the residue theorem	32
VI.	THE NODAL SOLUTION	41
	A. Introduction	41
	B. Development of the 3-D Model Equations	42
	C. Generating Input Data	59
	D. Source Representation	60
VII.	RESULTS AND ANALYSIS	62
	A. The Nodal Code Results	62
	B. The Analytical Solution	71
	C. Comparison of the Results	72
VIII.	CONCLUSION	88
IX.	SUGGESTIONS FOR FUTURE WORK	90
X.	LITERATURE CITED	92
XI.	ACKNOWLEDGMENTS	96

XII. APPENDIX A: THE NODAL CODE 97

A. Input Data Description 98

B. Input Data Generating Program 99

C. Sample Input File 101

D. Sample Output File 102

XIII. APPENDIX B: THE COMPUTER PROGRAM FOR THE ANALYTICAL SOLUTION 103

A. Input Data Description 105

B. Program Listing 107

C. Sample Input File 113

LIST OF TABLES

		PAGE
Table 4.1.	Two-group constants	20
Table 7.1.	The execution time of the nodal code on the National Advanced System/9160 computer (NAS)	69

LIST OF FIGURES

		PAGE
Figure 4.1.	The three-dimensional reactor model	22
Figure 5.1.	The differential volume in ξ space	33
Figure 5.2.	Fast real flux at mesh point (35,40,45) with source located at (50,50,50) and frequency of 10 rad/s calculated using all three analytical solution formulations	37
FIgure 5.3.	Thermal real flux at mesh point (35,40,45) with source located at (50,50,50) and frequency of 10 rad/s calculated using all three analytical solution formulations	38
Figure 5.4.	Fast imaginary flux at mesh point (35,40,45) with source located at (50,50,50) and frequency of 10 rad/s calculated using all three analytical solution formulations	39
Figure 5.5.	Thermal imaginary flux at mesh point (35,40,45) with source located at (50,50,50) and frequency of 10 rad/s calculated using all three analytical solution formulations	40
Figure 6.1.	The three-dimensional nodal geometry	43
Figure 6.2.	The average node flux at $x = \mp\eta$	48
Figure 6.3.	The point source representation in the nodal model	61
Figure 7.1.	The real component of the fast flux in the X-Y plane at Z=50 cm, ω=10 rad/s, and number of nodes =216	64
Figure 7.2.	The real component of the thermal flux in the X-Y plane at Z=50 cm, ω =10 rad/s, and number of nodes =216	65
Figure 7.3.	The imaginary component of the fast flux in the X-Y plane at Z=50 cm, ω =10 rad/s, and number of nodes =216	66

Figure 7.4.	The imaginary component of the thermal flux in the X-Y plane at Z=50 cm, ω =10 rad/s, and number of nodes =216	67
Figure 7.5.	Magnitude and phase of the zero power reactor transfer function, (ℓ/β)=1.9E-3 s	68
Figure 7.6.	Locations inside the cube used to compare the nodal results with the analytical solution of the frequency dependent neutron diffusion equations	75
Figure 7.7.	Ratio of analytical solution to nodal solution of the real fast flux at ω = 10 rad/s	76
Figure 7.8.	Ratio of analytical solution to nodal solution of the real thermal flux at ω = 10 rad/s	77
Figure 7.9.	Ratio of analytical solution to nodal solution of the imaginary fast flux at ω = 10 rad/s	78
Figure 7.10.	Ratio of analytical solution to nodal solution of the imaginary thermal flux at ω = 10 rad/s	79
Figure 7.11.	Ratio of analytical solution to nodal solution of the real fast flux at ω = .05 rad/s	80
Figure 7.12.	Ratio of analytical solution to nodal solution of the real thermal flux at ω = .05 rad/s	81
Figure 7.13.	Ratio of analytical solution to nodal solution of the imaginary fast flux at ω = .05 rad/s	82
Figure 7.14.	Ratio of analytical solution to nodal solution of the imaginary thermal flux at ω = .05 rad/s	83
Figure 7.15.	Ratio of analytical solution to nodal solution of the real fast flux at ω = 1000 rad/s	84

Figure 7.16. Ratio of analytical solution to nodal solution of the real thermal flux at ω = 1000 rad/s 85

Figure 7.17. Ratio of analytical solution to nodal solution of the imaginary fast flux at ω = 1000 rad/s 86

Figure 7.18. Ratio of analytical solution to nodal solution of the imaginary thermal flux at ω = 1000 rad/s 87

Figure B.1. Location of B_g, the roots of equation 5.21, at different frequencies 104

I. INTRODUCTION

Reactor noise analysis can have a significant role in the diagnosis of nuclear power plant malfunctions and in monitoring the general kinetic behavior of the reactor. It has the advantage of detection and measurement while the reactor is in operation. Since there are several sources of power reactor noise, it is a challenging task to identify and locate the noise sources without interfering with reactor performance. One category of these noise sources is the mechanical vibration of reactor components such as the vibration of control rods, fuel elements and core assemblies due to excitation by coolant flow (46).

Reactor noise as a phenomenon has been studied experimentally and theoretically. Moreover, noise measurement techniques have been applied to improve the safety and the availability of nuclear power plants (23). One of the theoretical approaches used in noise analysis is the adjoint formulation (1, 5, 9, 13, 14, 15, 18, 24, 27, 40). The technique requires the knowledge of the detector adjoint function for a certain perturbation and detector position combination. This information is used to determine detector response, its auto power spectral density, and the coherence function for various combination of detectors signals.

The objective of this research is to develop a three-dimensional numerical procedure that can be used in calculating the frequency-dependent detector adjoint function.

II. LITERATURE REVIEW

Neutron fluctuations due to absorber rod vibration have been investigated by several authors. One of the early studies on this subject was performed by Weinberg and Schweinler (44). Their work was mathematically rigorous (12) but the results were too intricate to be used for diagnostics (27). They investigated the response of a critical reactor to an oscillating thermal neutron absorber placed inside the core. The fluctuating neutron flux equations were derived and a series form solution was obtained. The solution was applied to the cases of an absorber of fluctuating strength distributed uniformly throughout the reactor, a localized absorber with a frequency which was below the period of delayed neutrons (below the break frequency of the zero power reactivity transfer function), and a localized absorber oscillating at a high frequency. For the first two cases, the vibrating absorber produced both space-independent fluctuations (long range component) and space-dependent fluctuations (short range component) in the neutron field in the neighborhood of the absorber due to the local depression movement. In these two cases, the solution was approximated by the first mode of the series solution. For the third case of high frequency oscillation, the reactivity effect disappeared, due to the low pass filter effect of the transfer function,

but the local depression remained with a broader frequency response. Moreover, the series solution converged poorly since the fundamental mode was no longer predominant. To increase the rate of convergence, they developed the solution by applying Poisson's summation formula (8) and the residue theorem. Consequently, this modification was expected to be more accurate and have better convergence properties. This paper is regarded as the basis for the idea of separating the neutron field induced by a localized perturbation into global and local components (2).

Cohn et al. (7) developed a method to calculate the source transfer function in the multigroup, multidimensional approximation, using a static technique. They resolved the time-dependent flux into steady and fluctuating components. A sinusoidal time-dependent source and flux response were assumed, then the two-group and time-dependent equations were transformed into a set of four complex equations in the frequency domain. The complex fluxes yield the gain and phase shift for each frequency of interest. They reported both numerical results and experimental data from the NORA reactor. The same analytical technique was adopted by Jeffers (19) and applied to an Argonaut type reactor using one-dimensional two-group diffusion theory. In analogy to Cohn et al. (7) and making use of the Green's function, Schwalm (39) solved the two-dimensional time-dependent

diffusion theory for a localized absorber. Basically his paper was about detecting failures in power reactors using noise measurements.

Compared to the model introduced by Weinberg and Schweinler (44), a simpler theoretical model was presented by Williams (45). He considered three basic problems, one was the case of a single point absorber randomly vibrating in a finite medium. He utilized the perturbation principle to find an equation for the change in reactivity due to the random vibration. The main concern of this paper was reactivity changes or global effects. This model was used by Kosály and Williams (20) in an attempt to interpret experimental results. They demonstrated that useful information regarding vibration of mechanical parts may be obtained by fitting the theoretical model to the experimental results.

Wach and Kosály (43) developed a simple space-dependent model to find the transfer function between two neutron detectors placed in the core of a large BWR. They distinguished between the local and global sources of reactor noise and also considered their joint effect. The model was supported later with theory (21) and related to diffusion theory.

The time-dependent importance (adjoint) function was defined by Lewins (26) as the expected contribution of any

neutron to a meter reading at an arbitrary time. The generalized adjoint space formulation taking into account the delayed neutrons was presented by Greenspan (13).

Based on the modified model reported by Kosály and Meskó (21) and the adjoint formulation reported by Greenspan (13), Dam (9) suggested an adjoint function technique to calculate the space and frequency-dependent transfer function which describes the relation between parametric fluctuations in a reactor and the response of neutron detectors to these fluctuations. He solved the system of frequency-dependent Langevin equations satisfied by the fluctuations of the fast and thermal fluxes. Dividing the frequency-dependent adjoint flux, a complex quantity, into real and imaginary parts, he obtained four equations. This set of four equations could be solved by any static numerical method that can handle four energy group fluxes, some of which may by negative. Hence, detector responses and the cross power spectral densities of several detectors positioned in the reactor can be obtained.

Using two-group diffusion theory, Behringer et al. (5) introduced a firm theoretical basis to the local and global concept of the neutron noise field. They followed the same adjoint technique presented by Dam (9) and found an expression for the adjoint flux. Since the aim of the paper was to provide a general theoretical background, a very

simplified model was used for analysis.

Pázsit (27) used a one-group model to solve the space-dependent diffusion equations for a vibrating weak absorber. He utilized the Green's function method suggested by Dam (9). Two cases were considered, the infinite, homogeneous medium and a bare homogeneous system with vacuum boundary conditions. He investigated the behavior of the auto power spectral densities at the plateau frequency for different reactor sizes and different absorber positions. The cross power spectral densities were not mentioned in this paper. The work was extended to two energy groups and to a two-region reactor (28). Moreover, the calculations indicated that in the frequency range of interest, the imaginary parts of the adjoint functions are very small compared to the real parts. The paper also presented an overall view of the theoretical approach.

The advantages of using the adiabatic-approximation rather than using the point-reactor model was the topic of a paper by Kosály and Meskó (21). They introduced the linear version of the adiabatic-approximation and investigated its validity in connection with the simple example of a localized absorber of variable strength. Although they used a one-group, one-dimensional model, they concluded that the adiabatic model was valid for small cores like the point-reactor model, was satisfactory for the intermediate size

systems, but did not hold for the large cores.

The adjoint formulation of transport theory was presented by Dam (10) and applied to power reactor noise identification and localization. The frequency-dependent transport equations were developed and the detector response to the isotropic source of neutrons was given. Also the auto power density of the detector fluctuations and the cross power spectral density of the signals from two neutron detectors were formulated.

Huang (18) outlined the derivation of the adjoint flux formulation and the detector response functions in the frequency domain. Restricting the frequency to the plateau region of the zero power transfer function, $\lambda << \omega << \beta/\ell$, he reduced the coefficients of the adjoint flux equations by approximating $\omega^2+\lambda^2$ with ω^2. This approximation is valid since the magnitude of the frequency is very large compared to the delayed neutrons decay constant. Consequently, the coupling between the real and imaginary flux equations was removed. Moreover, he neglected the imaginary parts of the adjoint fluxes since they were small in magnitude and derived a simple detector response formulation.

The reactor noise analysis review papers (4, 6, 22, 36, 37, 38, 41), presented a good link between the theoretical models and practical applications of noise analysis in nuclear reactors. Moreover, they gave an overall view of

the validity and restrictions imposed on the theory.

Most of the previously mentioned references were restricted to one-dimensional modeling. The models have been used to explain several characteristics of the neutron noise induced by random rod vibrations but they could not be applied directly to physical situations. Pázsit and Analytis (29) solved the modified one-group diffusion equations with an appropriate slowing down kernel and the two-group diffusion equations over rectangular coordinates. They neglected the imaginary parts of the frequency-dependent equations and used the Green's functions for the case of a control rod vibration in a bare reactor.

Al-Ammar (1) derived the detector response to a vibrating absorber using two neutron energy groups and the adjoint formulation. He also developed a one-dimensional code to calculate the frequency-dependent detector response function for the Iowa State University UTR-10 nuclear reactor.

Localization of reactor malfunctions with neutron noise techniques is possible only if the noise is space-dependent within the frequency range of interest. Several authors (3, 11, 35) have investigated the appropriate frequency ranges and core dimensions. Using the one-group diffusion model and expanding the Green's function into the orthonormal spatial eigenfunctions of the Helmholtz equations, Saito and

Otsuka (35) concluded that for almost all cores of practical interest, the Green's function and its Laplace transform (the system transfer function) may be well defined by the fundamental term, at least for frequencies smaller than β/ℓ. Edelmann (11) showed that for fast reactors, the frequency and space dependence of the transfer function can be separated only for $\omega < \beta/\ell$. Typical values of β/ℓ are 10^2 s^{-1} for thermal reactors and 10^3 - 10^4 s^{-1} for fast reactors (3). Following Saito and Otsuka (35), Antonopoulos-Domis (3) concluded that for a bare, homogeneous, large reactor, significant deviation from the point reactor model occurred at frequencies below β/ℓ only if the detector was near the perturbation. He defined large reactors as large in a migration length sense and not necessarily in physical size.

Multigroup modeling of random neutron noise was investigated by Analytis (2) and Lee (25). The authors proved the validity of the model and verified the local-global concept. Using the three-group, three-dimensional time-dependent linearized stochastic neutron diffusion equations for small fluctuations in the neutronic parameters, it was shown (2) that the neutron noise in a finite homogeneous reactor can be separated into three components. One of these components was defined as the global component while the other two were defined as the local components. Moreover, it was concluded that for a G-

group diffusion theory analysis of neutron noise in a homogeneous medium, there will be one global and G-1 local components. This is the same conclusion achieved by Lee (25).

Gotoh and Yasuda (12) studied the space-dependent neutron flux fluctuations excited by a strong absorber, applying one-dimensional one-group diffusion theory. The study was a simulation of a sudden displacement of an absorber in a reactor. They showed that the flux depression around the absorber rapidly follows the displacement of the absorber, but there is some time delay before the fluctuation effect reaches the steady flux at regions farther from the absorber.

Pázsit and Glöckler (30, 31) proposed a vibrating control rod monitoring technique. The space-dependent neutron noise is induced by two-dimensional vibration of a control rod. The authors described a procedure by which equilibrium rod position and trajectory or displacement component characteristics can be determined from signals of as few as three detectors. Investigation considered both periodic vibrations (30) and stochastic vibrations (31).

The diagnostic problem of two-dimensional control rod vibration in a PWR using the measurable power spectral densities of an in-core neutron detector was studied analytically by Lee and Albrecht (24). Based on two-group

diffusion theory for a reflected reactor, the frequency-dependent Langevin equations were derived. The adjoint function technique was applied to obtain the frequency response to a control rod vibration. In the plateau region they studied the frequency response as a function of detector position and location of the absorber rod. They introduced a "contour" concept (points with equal response for vibrations at a certain location) to locate a vibrating rod and to estimate the root-mean-square vibration amplitude.

The response of a nuclear reactor to a moving absorber was investigated recently by Hennessy (14) and Hennessy et al. (15). The response (in terms of the Auto Power Spectral Density of the neutron detector) as a function of separation distance from a vibrating source has been compared with the response predicted by a two-dimensional two-group model of the UTR-10 nuclear reactor at Iowa State University. The coherence functions for various combination of detector signals and phase shift between detectors were also used to interpret the response.

Sweeney and Renier (40) calculated the frequency-dependent detector response using both the TASK and JPRKINETICS computer codes. The TASK code can be used to solve the space, energy, and frequency-dependent Boltzmann equations with delayed neutrons. The TASK computer code can

solve one-dimensional slab, frequency-dependent discrete ordinates detector adjoint equations with delayed neutrons. The JPRKINETICS code solves a two-dimensional frequency-dependent diffusion theory detector adjoint equations with delayed neutrons. The numerical results were compared with the experimental ex-core neutron noise data obtained from the Sequoyah-1 pressurized water reactor.

III. DEVELOPING THE EQUATIONS

In this chapter, the Fourier transformed diffusion equations are developed for a general multigroup model. From this model, a special case of two neutron energy groups is considered for investigation and analysis.

The time-dependent multigroup neutron diffusion equations with delayed neutrons are (16)

$$\frac{\partial}{\partial t}\left(\frac{\phi_g(\underline{r},t)}{v_g}\right) = \nabla\cdot\left(D_g(\underline{r},t)\nabla\phi_g(\underline{r},t)\right)$$

$$- \Sigma_{tg}(\underline{r},t)\phi_g(\underline{r},t)$$

$$+ (1-\beta)\chi_{pg}\sum_{g'}\nu\Sigma_{fg'}(\underline{r},t)\phi_{g'}(\underline{r},t)$$

$$+ \sum_{g'}\Sigma_{gg'}(\underline{r},t)\phi_{g'}(\underline{r},t)$$

$$+ \sum_{i}\chi_{ig}\lambda_i C_i(\underline{r},t) \qquad (3.1)$$

$$\frac{\partial C_i(\underline{r},t)}{\partial t} = \beta_i\sum_{g'}\nu\Sigma_{fg'}(\underline{r},t)\phi_{g'}(\underline{r},t) - \lambda_i C_i \qquad (3.2)$$

Starting with a source free steady state reactor, (k=1), a small perturbation is introduced in the group absorption cross section, which will induce fluctuations in the group fluxes [$\phi_g(\underline{r},t)$] and in the delayed neutron

precursor concentrations $[C_i(\underline{r},t)]$. Thus, one can introduce the following expressions:

$$\Sigma_{tg}(\underline{r},t) = \Sigma_{tg}(\underline{r}) + \delta\Sigma_{tg}(\underline{r},t) \tag{3.3}$$

$$\phi_g(\underline{r},t) = \phi_g(\underline{r}) + \delta\phi_g(\underline{r},t) \tag{3.4}$$

$$C_i(\underline{r},t) = C_i(\underline{r}) + \delta C_i(\underline{r},t) \tag{3.5}$$

where $\Sigma_{tg}(\underline{r})$, $\phi_g(\underline{r})$ and $C_i(\underline{r})$ are the steady state components and $\delta\Sigma_{tg}(\underline{r},t)$, $\delta\phi_g(\underline{r},t)$ and $\delta C_i(\underline{r},t)$ are the perturbation components.

Substituting equations (3.3), (3.4) and (3.5) into equations (3.1) and (3.2), dropping steady state terms, linearizing by neglecting second order terms and omitting the functional dependence for convenience, one obtains

$$\frac{1}{v_g}\frac{\partial}{\partial t}\delta\phi_g = D_g\nabla^2\delta\phi_g - \Sigma_{tg}\delta\phi_g - \delta\Sigma_{tg}\phi_g$$
$$+ (1-\beta)\chi_{pg}\sum_{g'}\nu\Sigma_{fg'}\delta\phi_{g'}$$
$$+ \sum_{g'}\Sigma_{gg'}\delta\phi_{g'} + \sum_{i}\chi_{ig}\lambda_i\delta C_i \tag{3.6}$$

$$\frac{\partial\delta C_i}{\partial t} = \beta_i\sum_{g'}\nu\Sigma_{fg'}\delta\phi_{g'} - \lambda_i\delta C_i \tag{3.7}$$

where $\delta\phi_g$, δC_i and $\delta\Sigma_{tg}$ are both space and time-dependent while D_g, ϕ_g, $\nu\Sigma_{fg'}$ and $\Sigma_{gg'}$ are only space-dependent.

Applying the Fourier transform

$$\Delta f_g(\underline{r},\omega) = \int_{-\infty}^{\infty} \delta f_g(\underline{r},t) \exp(-j\omega t)\, dt \tag{3.8}$$

to equations (3.6) and (3.7) one obtains

$$\frac{1}{v_g} j\omega\Delta\phi_g = D_g\nabla^2\Delta\phi_g - \Sigma_{tg}\Delta\phi_g - \Delta\Sigma_{tg}\phi_g$$

$$+ (1-\beta)\chi_{pg} \sum_{g'} \nu\Sigma_{fg'}\Delta\phi_{g'}$$

$$+ \sum_{g'} \Sigma_{gg'}\Delta\phi_{g'} + \sum_{i} \chi_{ig}\lambda_i\Delta C_i \tag{3.9}$$

$$j\omega\Delta C_i = \beta_i \sum_{g'} \nu\Sigma_{fg'}\Delta\phi_{g'} - \lambda_i\Delta C_i \tag{3.10}$$

where $\Delta\phi_g$, ΔC_i and $\Delta\Sigma_{tg}$ are functions of space and frequency. The fluctuation in the delayed neutron precursor concentration can be found from equation (3.10) and can be replaced in equation (3.9) as follows,

$$\Delta C_i = \frac{\beta_i \sum_{g'} \nu\Sigma_{fg'}\Delta\phi_{g'}}{\lambda_i + j\omega} \tag{3.11}$$

Therefore, equation (3.9) is changed to,

$$D_g\nabla^2\Delta\phi_g - \frac{\omega}{v_g}j\Delta\phi_g - \Sigma_{tg}\Delta\phi_g$$

$$+ (1-\beta)\chi_{pg}\sum_{\acute{g}}\nu\Sigma_{f\acute{g}}\Delta\phi_{\acute{g}} + \sum_{\acute{g}}\Sigma_{g\acute{g}}\Delta\phi_{\acute{g}}$$

$$+ \sum_i\left(\frac{\chi_{ig}\lambda_i\beta_i}{\lambda_i+j\omega}\sum_{\acute{g}}\nu\Sigma_{f\acute{g}}\Delta\phi_{\acute{g}}\right) = \Delta\Sigma_{tg}\phi_g \qquad (3.12)$$

Since the Fourier transformed group flux fluctuation terms are complex quantities, they can be separated into real and imaginary parts

$$\Delta\phi_g = \Psi_g + X_g j \qquad (3.13)$$

Inserting equation (3.13) into equation (3.12) and separating real and imaginary quantities one obtains,

$$D_g\nabla^2\Psi_g - \Sigma_{tg}\Psi_g - \Delta\Sigma_{tg}\phi_g$$

$$+ (1-\beta)\chi_{pg}\sum_{\acute{g}}\nu\Sigma_{f\acute{g}}\Psi_{\acute{g}} + \sum_{\acute{g}}\Sigma_{g\acute{g}}\Psi_{\acute{g}}$$

$$+ \sum_i\frac{\chi_{ig}\lambda_i^2\beta_i\sum_{\acute{g}}\nu\Sigma_{f\acute{g}}\Psi_{\acute{g}} + \omega\chi_{ig}\lambda_i\beta_i\sum_{\acute{g}}\nu\Sigma_{f\acute{g}}X_{\acute{g}}}{(\lambda_i^2+\omega^2)} = -\frac{\omega}{v_g}X_g$$

(3.14)

$$D_g\nabla^2 X_g - \Sigma_{tg}X_g + (1-\beta)\chi_{pg}\sum_{g'}\nu\Sigma_{fg'}X_{g'} + \sum_{g'}\Sigma_{gg'}X_{g'} + \sum_i \frac{\chi_{ig}\lambda_i^2\beta_i\sum_{g'}\nu\Sigma_{fg'}X_{g'} - \omega\chi_{ig}\lambda_i\beta_i\sum_{g'}\nu\Sigma_{fg'}\Psi_{g'}}{(\lambda_i^2+\omega^2)} = \frac{\omega}{v_g}\Psi_g \qquad (3.15)$$

Thus, one gets a set of 2N coupled nonhomogeneous frequency and space-dependent equations where N is the number of multigroup equations. These equations can be solved for a single frequency value for a given geometry by appropriate static computer codes that can handle an equivalent multigroup problem.

The following approximations were imposed on the multigroup, frequency-dependent diffusion equations :

1) The analysis was based on two neutron energy groups which yield four coupled set of equations.
2) One delayed neutron group was assumed.
3) Perturbations were in the thermal absorption cross section only.

Therefore, equations (3.14) and (3.15) were reduced to

$$D_1\nabla^2\Psi_1 - (\Sigma_{a1}+\Sigma_{21}-\nu\Sigma_{f1}H_R)\Psi_1 + (\nu\Sigma_{f2}H_R)\Psi_2$$

$$+ (\frac{\omega}{v_1} -\nu\Sigma_{f1}H_I)X_1 - (\nu\Sigma_{f2}H_I)X_2 = 0 \qquad (3.16)$$

$$D_2\nabla^2\Psi_2 - (\Sigma_{a2})\Psi_2+(\Sigma_{21})\Psi_1 + \frac{\omega}{v_2}X_2 = \Delta\Sigma_{a2}\phi_2 \qquad (3.17)$$

$$D_1\nabla^2X_1 - (\Sigma_{a1}+\Sigma_{21}-\nu\Sigma_{f1}H_R)X_1 - (\frac{\omega}{v_1} -\nu\Sigma_{f1}H_I)\Psi_1$$

$$+ (\nu\Sigma_{f2}H_I)\Psi_2 + (\nu\Sigma_{f2}H_R)X_2 = 0 \qquad (3.18)$$

$$D_2\nabla^2X_2 - (\Sigma_{a2})X_2 - \frac{\omega}{v_2}\Psi_2+\Sigma_{21}X_1 = 0 \qquad (3.19)$$

where

$$H = H_R + jH_I \qquad (3.20)$$

$$H_R= \frac{\lambda^2 + \omega^2(1-\beta)}{\lambda^2+\omega^2} \qquad (3.21)$$

$$H_I= - \frac{\omega\lambda\beta}{\lambda^2+\omega^2} \qquad (3.22)$$

IV. THE REACTOR MODEL

Since the main goal of this research was to develop and prove the validity of nodal solution methods for the frequency-dependent flux equations 3.16 - 3.19, a simple three-dimensional cubic reactor geometry was chosen, see Figure 4.1. Moreover, the reactor was assumed homogeneous with homogeneous boundary conditions. The two neutron energy group material properties were taken from the three-dimensional IAEA benchmark problem specification (42). The thermal group fission cross section was altered to assure the criticality of the system before the perturbation. The side of the cube was taken as 100 centimeters. The two-group parameters are listed in Table 4.1.

Table 4.1. Two-group constants

Parameter		Group (1)	Group (2)
D	cm	1.5	0.4
Σ_a	cm^{-1}	0.01	0.08
$\nu\Sigma_f$	cm^{-1}	0.00	0.14
Σ_R	cm^{-1}	0.02	0.00
χ		1.00	0.00
v	cm/s	3.6E6	2.2E5

Other parameters used were β = 0.0065 and λ = 0.1 s^{-1}. In addition, using the two-group constants and following Hetrick (17), the neutron generation time was calculated for the critical reactor model as ℓ = 1.234E-5 s.

For analysis, the perturbation was assumed to be only in the thermal absorption cross section and confined to the center of the cube.

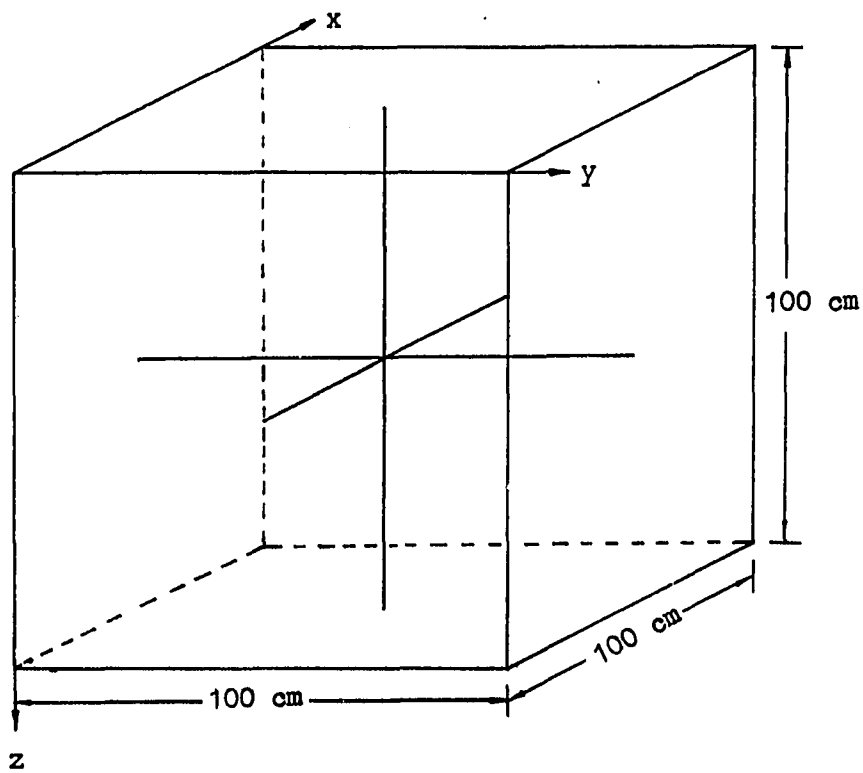

Figure 4.1. The three-dimensional reactor model

V. THE ANALYTICAL SOLUTION

In order to check the validity of the nodal model solution, an analytical model was developed. Both models were tested for the same reactor geometry and material composition.

A. Solution Development

Considering two neutron energy groups and a one delayed neutron precursor group, ignoring upscattering and assuming a perturbation in the thermal absorption cross section alone, equation (3.12) is reduced to the following,

$$D_1\nabla^2\Delta\phi_1 - (\Sigma_{a1}+\Sigma_{21})\Delta\phi_1 + (1-\beta)\chi_1(\nu\Sigma_{f1}\Delta\phi_1+\nu\Sigma_{f2}\Delta\phi_2)$$

$$+ \frac{\chi_1\lambda\beta}{\lambda+j\omega}(\nu\Sigma_{f1}\Delta\phi_1+\nu\Sigma_{f2}\Delta\phi_2) - \frac{j\omega}{v_1}\Delta\phi_1 = 0 \qquad (5.1)$$

$$D_2\nabla^2\Delta\phi_2 - (\Sigma_{a2})\Delta\phi_2 + (\Sigma_{21})\Delta\phi_1$$

$$+ (1-\beta)\chi_2(\nu\Sigma_{f1}\Delta\phi_1+\nu\Sigma_{f2}\Delta\phi_2)$$

$$+ \frac{\chi_2\lambda\beta}{\lambda+j\omega}(\nu\Sigma_{f1}\Delta\phi_1+\nu\Sigma_{f2}\Delta\phi_2) - \frac{j\omega}{v_2}\Delta\phi_2 = \Delta\Sigma_{a2}\phi_2 \qquad (5.2)$$

where $\Delta\phi_1$ and $\Delta\phi_2$ are the complex space and frequency-dependent fluctuations in the fast and the thermal fluxes.

Following Weinberg and Schweinler (44), the flux fluctuation is expanded in eigenfunctions of the Helmholtz

equation $\nabla^2\phi + B^2\phi = 0$ subject to zero boundary conditions.

$$\Delta\phi_g = \sum_{l,m,n=1}^{\infty} A_{lmng}\, W_{lmn} \tag{5.3}$$

where

$$W_{lmn} = \left(\frac{8}{abc}\right)^{1/2} \sin\left(\frac{l\pi x}{a}\right) \sin\left(\frac{m\pi y}{b}\right) \sin\left(\frac{n\pi z}{c}\right) \tag{5.4}$$

and

$$\int_0^a \int_0^b \int_0^c W_{lmn}^2 \, dz\, dy\, dx = 1 \tag{5.5}$$

where a, b and c are reactor dimensions. Also from equation (5.3) one can get,

$$\nabla^2\Delta\phi_g = \sum_{l,m,n=1}^{\infty} (-A_{lmng}\, B_{lmn}^2\, W_{lmn}) \tag{5.6}$$

where

$$\underline{B}_{lmn} = \left(\frac{l\pi}{a}\right)\underline{i} + \left(\frac{m\pi}{b}\right)\underline{j} + \left(\frac{n\pi}{c}\right)\underline{k} \tag{5.7}$$

substituting equations (5.3) and (5.6) into equations (5.1) and (5.2) one gets,

$$D_1 \sum_{l,m,n=1}^{\infty} (-A_{lmn1}B_{lmn}^2 W_{lmn}) + G_1 \sum_{l,m,n=1}^{\infty} (A_{lmn1}W_{lmn})$$

$$+ G_2 \sum_{l,m,n=1}^{\infty} (A_{lmn2}W_{lmn}) = 0 \qquad (5.8)$$

and

$$D_2 \sum_{l,m,n=1}^{\infty} (-A_{lmn2}B_{lmn}^2 W_{lmn}) + G_3 \sum_{l,m,n=1}^{\infty} (A_{lmn1}W_{lmn})$$

$$+ G_4 \sum_{l,m,n=1}^{\infty} (A_{lmn2}W_{lmn}) = \Delta\Sigma_{a2}\phi_2 \, \delta(x-x_0)\delta(y-y_0)\delta(z-z_0) \qquad (5.9)$$

where $\delta(x-x_0)\delta(y-y_0)\delta(z-z_0)$ is the three-dimensional Dirac delta function used to represent the perturbation in the thermal group absorption cross section at the location (x_0, y_0, z_0)

and

$$G_1 = -\Sigma_{a1} - \Sigma_{21} + (1-\beta)\nu\Sigma_{f1} + \frac{\lambda\beta\nu\Sigma_{f1}}{\lambda+j\omega} - j\frac{\omega}{v_1} \qquad (5.10)$$

$$G_2 = (1-\beta)\nu\Sigma_{f2} + \frac{\lambda\beta\nu\Sigma_{f2}}{\lambda+j\omega} \tag{5.11}$$

$$G_3 = \Sigma_{21} \tag{5.12}$$

$$G_4 = -\Sigma_{a2} - \frac{\omega}{v_2}\, j \tag{5.13}$$

Multiplying equations (5.8) and (5.9) by (W_{1mn}), integrating over the reactor volume and making use of equation (5.5) and the orthogonality of the eigenfunctions, one obtains,

$$G_1A_{1mn1} + G_2A_{1mn2} - D_1B_{1mn}^2A_{1mn1} = 0 \tag{5.14}$$

$$G_3A_{1mn1} + G_4A_{1mn2} - D_2B_{1mn}^2A_{1mn2}$$

$$= \Delta\Sigma_{a2}\phi_2 \left(\frac{8}{abc}\right)^{1/2} \sin\left(\frac{l\pi x_0}{a}\right) \sin\left(\frac{m\pi y_0}{b}\right) \sin\left(\frac{n\pi z_0}{c}\right) \tag{5.15}$$

which can be solved for A_{1mn1} and A_{1mn2}

$$A_{1mn1} = \frac{\Delta\Sigma_{a2}\phi_2(8/abc)^{1/2}\sin(l\pi x_0/a)\sin(m\pi y_0/b)\sin(n\pi z_0/c)}{[G_3G_2+(G_4-D_2B_{1mn}^2)(D_1B_{1mn}^2-G_1)]/G_2} \tag{5.16}$$

$$A_{1mn2} = \frac{\Delta\Sigma_{a2}\phi_2(8/abc)^{1/2}\sin(l\pi x_0/a)\sin(m\pi y_0/b)\sin(n\pi z_0/c)}{[G_3G_2+(G_4-D_2B_{1mn}^2)(D_1B_{1mn}^2-G_1)]/(D_1B_{1mn}^2-G_1)} \tag{5.17}$$

substituting equations (5.16) and (5.17) into equation (5.3) one obtains.

$$\Delta\phi_1 = \Delta\Sigma_{a2}\phi_2\left(\frac{8}{abc}\right)\sum_{l,m,n=1}^{\infty}\frac{Z(x_0,y_0,z_0,x,y,z)}{P_1} \tag{5.18}$$

$$\Delta\phi_2 = \Delta\Sigma_{a2}\phi_2\left(\frac{8}{abc}\right)\sum_{l,m,n=1}^{\infty}\frac{Z(x_0,y_0,z_0,x,y,z)}{P_2} \tag{5.19}$$

where

$$Z(x_0,y_0,z_0,x,y,z) = \sin\left(\frac{l\pi x}{a}\right)\sin\left(\frac{l\pi x_0}{a}\right)\sin\left(\frac{m\pi y}{b}\right)\sin\left(\frac{m\pi y_0}{b}\right)\sin\left(\frac{n\pi z}{c}\right)\sin\left(\frac{n\pi z_0}{c}\right) \tag{5.20}$$

$$P = [(-D_1D_2)B_{lmn}^4+(D_1G_4+D_2G_1)B_{lmn}^2+(G_3G_2-G_1G_4)] \tag{5.21}$$

$$P_1 = P/G_2 \tag{5.22}$$

$$P_2 = P/(D_1B_{lmn}^2-G_1) \tag{5.23}$$

$$B_{lmn}^2 = \left(\frac{l\pi}{a}\right)^2 + \left(\frac{m\pi}{b}\right)^2 + \left(\frac{n\pi}{c}\right)^2 \tag{5.24}$$

and G_1, G_2, G_3 and G_4 were defined in equations 5.10, 5.11, 5.12 and 5.13.

B. Modifying the Solution

As reported by Weinberg and Schweinler (44), the triple sine summation solution is a poorly converging series. Therefore, a modification is required in order to get a reliable solution that is accurate and better converging. They suggested the use of the Poisson's summation formulation (8) which is applied in the following section.

The sine terms in equation (5.20) can be replaced by their exponential form according to the following equation,

$$\sin(\theta) = \frac{\exp(j\theta) - \exp(-j\theta)}{2j} \tag{5.25}$$

and the summation part of equation (5.20) will become

$$\sum_{l,m,n=1}^{\infty} Z(x_0,y_0,z_0,x,y,z)$$

$$= \sum_{l,m,n=1}^{\infty} \left(\frac{\exp(x^-)-\exp(x^+)-\exp(-x^+)+\exp(-x^-)}{4} \right.$$

$$\frac{\exp(y^-)-\exp(y^+)-\exp(-y^+)+\exp(-y^-)}{4}$$

$$\left. \frac{\exp(z^-)-\exp(z^+)-\exp(-z^+)+\exp(-z^-)}{4} \right) \tag{5.26}$$

where

$$x^+ = \left(\frac{jl\pi}{a}\right)(x+x_0)$$

$$x^- = \left(\frac{jl\pi}{a}\right)(x-x_0)$$

$$y^+ = \left(\frac{jm\pi}{b}\right)(y+y_0) \qquad (5.27)$$

$$y^- = \left(\frac{jm\pi}{b}\right)(y-y_0)$$

$$z^+ = \left(\frac{jn\pi}{c}\right)(z+z_0)$$

$$z^- = \left(\frac{jn\pi}{c}\right)(z-z_0)$$

1. Applying the Poisson's summation formula

The Poisson's summation formula in three-dimensions (8) is

$$\sum_{l,m,n} \phi(l,m,n)$$

$$= \sum_{\lambda,\mu,\nu} \iiint_{-\infty}^{\infty} \phi(u,v,w) \exp[-2\pi j(\lambda u+\mu v+\nu w)]\, du\, dv\, dw \qquad (5.28)$$

where l, m, n, λ, μ and ν take on all integer values from $-\infty$ to ∞. This formula is valid if all the integrals on the right exist, if

$$\sum_{l,m,n=-\infty}^{\infty} \phi(l+x,m+y,n+z)$$

converges uniformly in x,y,z for $0 \leq x,y,z < 2\pi$, and if this series represent a function which can be expanded in a Fourier series (8).

The aim now is to convert the summation of equation (5.26) to a form similar to the LHS of equation (5.28), then developing the RHS of equation (5.28) such that the integration can be performed analytically and the summation converges for a reasonable number of modes.

Performing some straightforward algebra, equation (5.26) can be expanded into 64 triple exponential terms

summed from 1 to ∞. The number of terms is reduced to eight triple summation terms by changing the summation limits to -∞ to ∞. Therefore equation (5.26) will have the following form,

$$\sum_{\lambda,\mu,\nu=-\infty}^{\infty} \frac{\exp[jl\pi(x\mp x_0)/a + jm\pi(y\mp y_0)/b + jn\pi(z\mp z_0)/c]}{64} \tag{5.29}$$

Introduce the following definitions

$$\bar{\xi} \equiv \frac{\pi u}{a}\,\underline{i} + \frac{\pi v}{b}\,\underline{j} + \frac{\pi w}{c}\,\underline{k} \tag{5.30}$$

$$d\bar{\xi} = \frac{\pi^3}{abc}\,du\,dv\,dw \tag{5.31}$$

$$\bar{R}_{\mp} \equiv (x\mp x_0)\,\underline{i} + (y\mp y_0)\,\underline{j} + (z\mp z_0)\,\underline{k} \tag{5.32}$$

$$\bar{\Lambda} \equiv 2\lambda a\,\underline{i} + 2\mu b\,\underline{j} + 2\nu c\,\underline{k} \tag{5.33}$$

Now the Poisson's summation formula is applied to equation (5.29) and substituted into equations (5.18) and (5.19), this will yield the following equations

$$\Delta\phi_1 = \Delta\Sigma_{a2}\phi_2\left(\frac{1}{8\pi^3}\right) \sum_{\lambda,\mu,\nu=-\infty}^{\infty} \iiint_{-\infty}^{+\infty} \sum_{i=1}^{8} \frac{\exp[j\bar{\xi}\cdot(\bar{R}_i-\bar{\Lambda})]}{P/G_2}\,d\xi \tag{5.34}$$

$$\Delta\phi_2 = \Delta\Sigma_{a2}\phi_2\left(\frac{1}{8\pi^3}\right) \sum_{\lambda,\mu,\nu=-\infty}^{\infty} \iiint_{-\infty}^{+\infty} \sum_{i=1}^{8} \frac{\exp[j\bar{\xi}\cdot(\bar{R}_i-\bar{\Lambda})]}{P/(D_1\xi^2{}_{1mn}-G_1)}\, d\xi \tag{5.35}$$

where the i stands for each of the 8 triple exponential summation terms of equation (5.29).

2. Applying the residue theorem

The integrals of equations (5.34) and (5.35) were evaluated by changing the geometric base to the spherical coordinate system and using the residue theorem. As shown in Figure 5.1, $\bar{\xi}$ is written as $\xi\bar{\Omega}$ where $\bar{\Omega}$ is a unit vector. The spherical coordinates were measured relative to the constant vector $\bar{R}-\bar{\Lambda}$. Considering the integral part of equation (5.34), where the same argument can be applied to equation (5.35), one has

$$I = \iiint_{-\infty}^{\infty} \frac{\exp[j\bar{\xi}\cdot(\bar{R}-\bar{\Lambda})]}{P/G_2}\, d\xi \tag{5.36}$$

where in the spherical coordinates,

$$d\bar{\xi} = \xi^2 \sin\theta\, d\theta\, d\phi\, d\xi \tag{5.37}$$

Then equation (5.36) will become

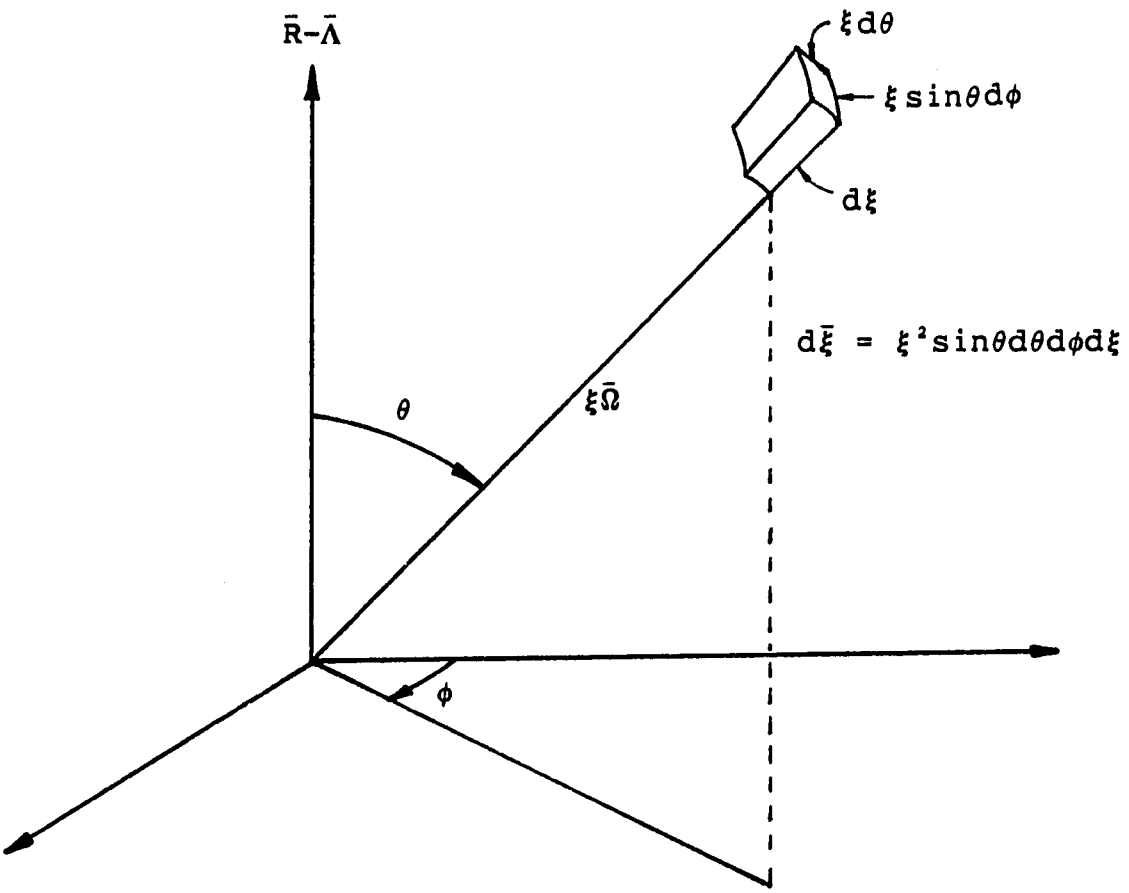

Figure 5.1. The differential volume in ξ space

$$I = \frac{2\pi}{j|R-\Lambda|}\int_{-\infty}^{\infty}\frac{\exp(j\xi|R-\Lambda|\cos\theta)}{P/G_2}\,\xi\,d\xi \tag{5.38}$$

Let B_s be the zeros with positive imaginary parts of P/G_2, which are also the poles of the integrand in equation (5.38). Then using the residue theorem and following a semicircular contour including the entire positive half plane, the value of the integral will be,

$$I = \frac{2\pi^2}{|R-\Lambda|}\left(\sum_s \frac{\exp(jB_s|R-\Lambda|)}{\left.\frac{d(P/G_2)}{d(\xi^2)}\right|_{B_s}}\right) \tag{5.39}$$

Thus the fast and thermal flux fluctuations will have the forms,

$$\Delta\phi_1 = \Delta\Sigma_{a2}\phi_2\left(\frac{1}{4\pi}\right)\sum_{\lambda,\mu,\nu}\sum_i \frac{1}{|R_i-\Lambda|}\left(\sum_s \frac{\exp(jB_s|R_i-\Lambda|)}{d[P/G_2]/d(\xi^2)|_{B_s}}\right) \tag{5.40}$$

$$\Delta\phi_2 = \Delta\Sigma_{a2}\phi_2\left(\frac{1}{4\pi}\right)\sum_{\lambda,\mu,\nu}\sum_i \frac{1}{|R_i-\Lambda|}\left(\sum_s \frac{\exp(jB_s|R_i-\Lambda|)}{d[P/(D_1\xi^2-G_1)]/(d\xi^2)|_{B_s}}\right) \tag{5.41}$$

where λ, μ and $\nu = -\infty$ to $+\infty$

and $i = 1, 2, \ldots, 8$

Weinberg and Schweinler (44) suggested a formulation

with only two triple exponential terms $\bar{R}_i$ and according to this formulation the fluxes have the following forms,

$$\Delta\phi_1 = \Delta\Sigma_{a2}\phi_2 \sum_{\lambda,\mu,\nu} \sum_{s} \frac{1}{d[P/G_2]/(d\xi^2)|_{B_s}} \left(\frac{\exp(jB_s R^-_{\lambda\mu\nu})}{4\pi R^-_{\lambda\mu\nu}} - \frac{\exp(jB_s R^+_{\lambda\mu\nu})}{4\pi R^+_{\lambda\mu\nu}} \right) \tag{5.42}$$

$$\Delta\phi_2 = \Delta\Sigma_{a2}\phi_2 \sum_{\lambda,\mu,\nu} \sum_{s} \frac{1}{d[P/(D_1\xi^2-G_1)]/(d\xi^2)|_{B_s}} \left(\frac{\exp(jB_s R^-_{\lambda\mu\nu})}{4\pi R^-_{\lambda\mu\nu}} - \frac{\exp(jB_s R^+_{\lambda\mu\nu})}{4\pi R^+_{\lambda\mu\nu}} \right) \tag{5.43}$$

where

$$R^- = [(x-x_0)^2+(y-y_0)^2+(z-z_0)^2]^{1/2} \tag{5.44}$$

$$R^+ = [(x+x_0)^2+(y+y_0)^2+(z+z_0)^2]^{1/2} \tag{5.45}$$

All three formulations of the analytical solution were tested and compared for several source locations, observation points, and different frequencies. The computer program used to obtain the analytical solution is presented in Appendix B. Figures 5.2 through 5.5 show the three solutions at the point (35,40,45) when ω = 10 rad/s, and with the source located at the point (50,50,50). The graphs

show the consistency between the eight triple exponential summation formulation and the triple sine summation formulation. The solution suggested by Weinberg and Schweinler (44) still requires the six remaining terms. The points at which the three formulations were tested were away from the source. At the center of the cube where the source is located, the solution never converges and keeps increasing as the number of modes increases. In the tested summation limits range, it was noticed that developing the solution using the Poisson's summation formula did not improve convergence but rather multiplied the computation effort required to get the same result calculated by the triple sine summation formulation.

Since the solution of the sine series form was proven to be the best representation of the analytical solution, it was chosen as the method to check the validity of the nodal solution of the frequency-dependent diffusion equations.

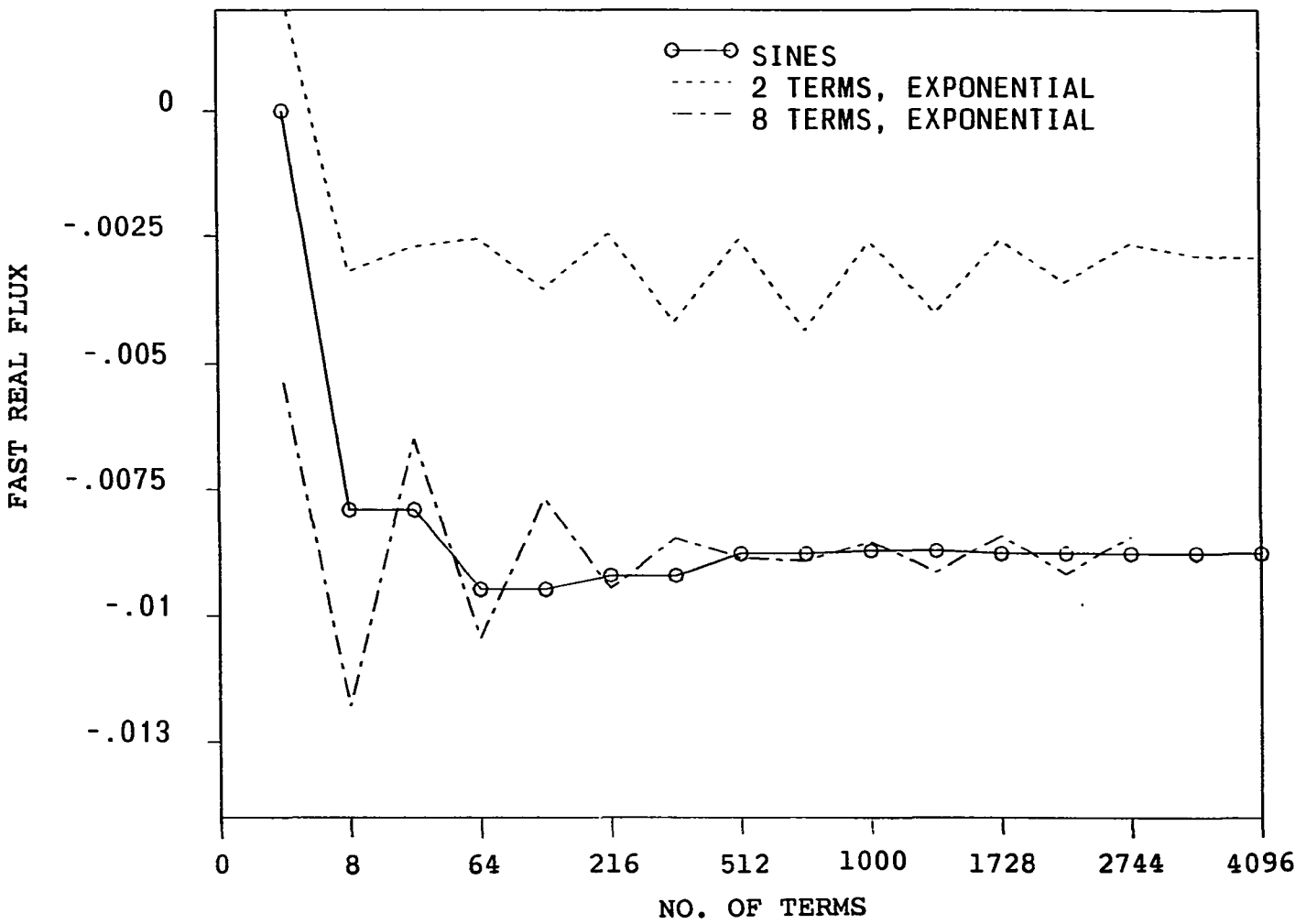

Figure 5.2. Fast real flux at mesh point (35,40,45) with source located at (50,50,50) and frequency of 10 rad/s calculated using all three analytical solution formulations

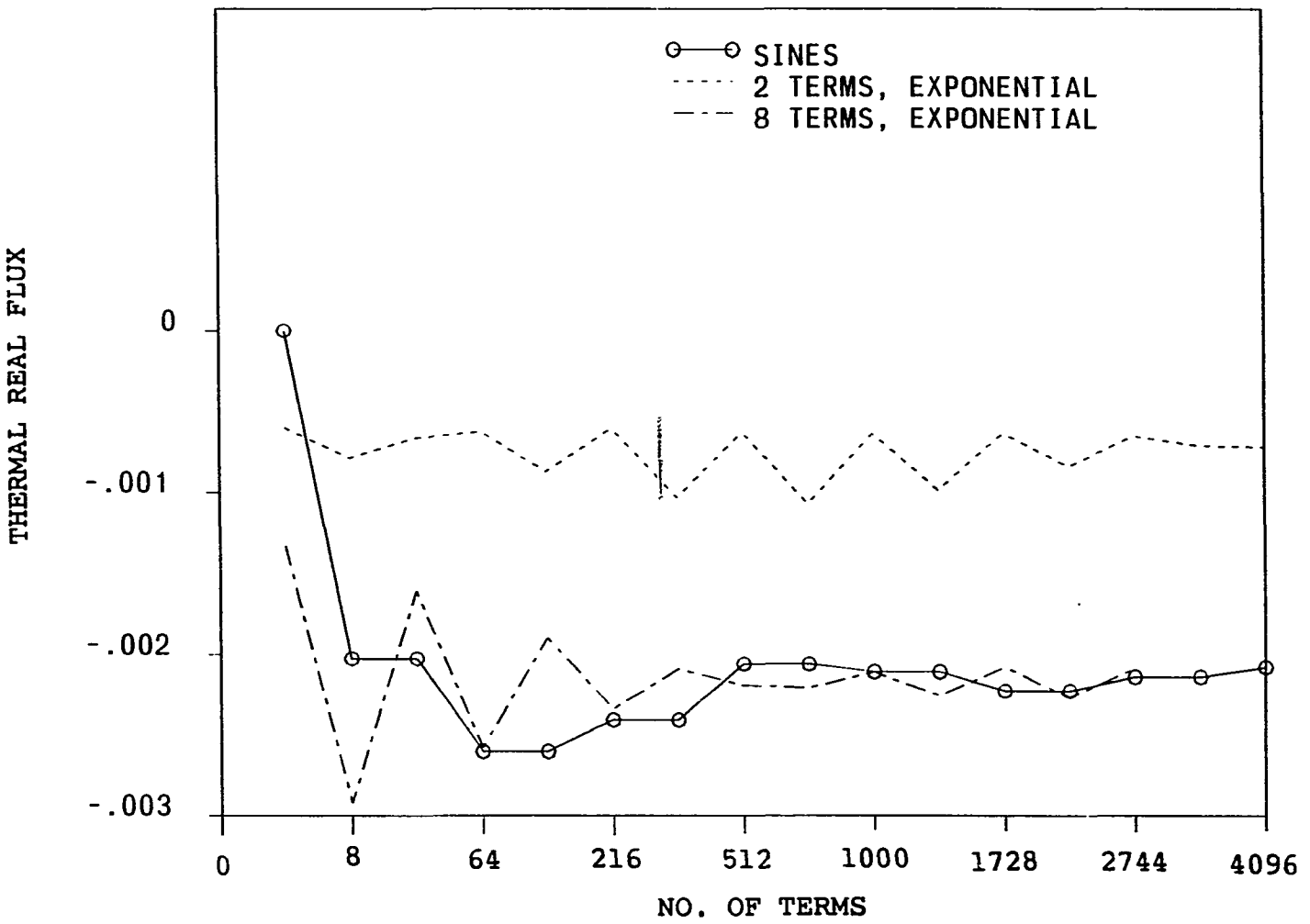

Figure 5.3. Thermal real flux at mesh point (35,40,45) with source located at (50,50,50) and frequency of 10 rad/s calculated using all three analytical solution formulations

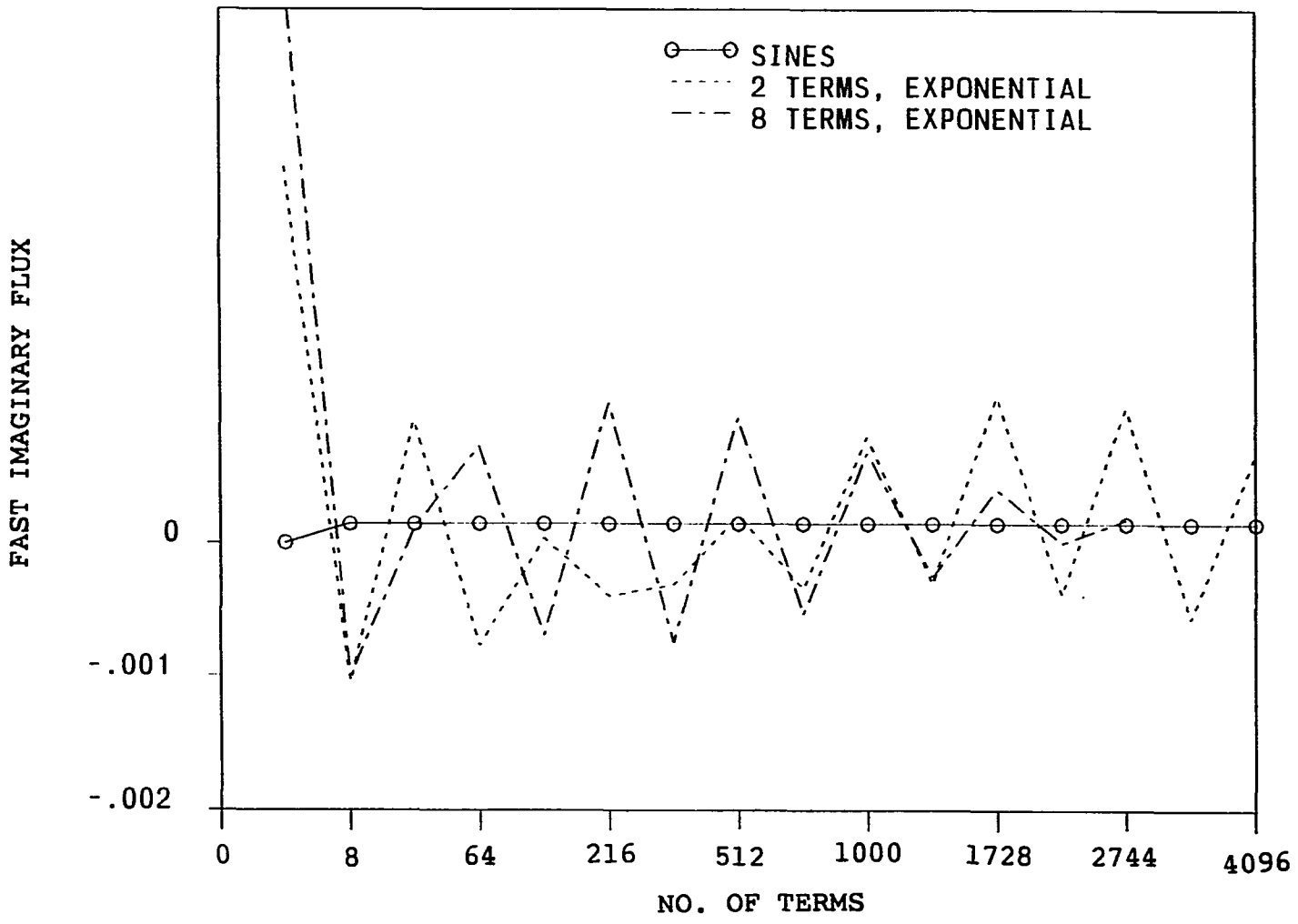

Figure 5.4. Fast imaginary flux at mesh point (35,40,45) with source located at (50,50,50) and frequency of 10 rad/s calculated using all three analytical solution formulations

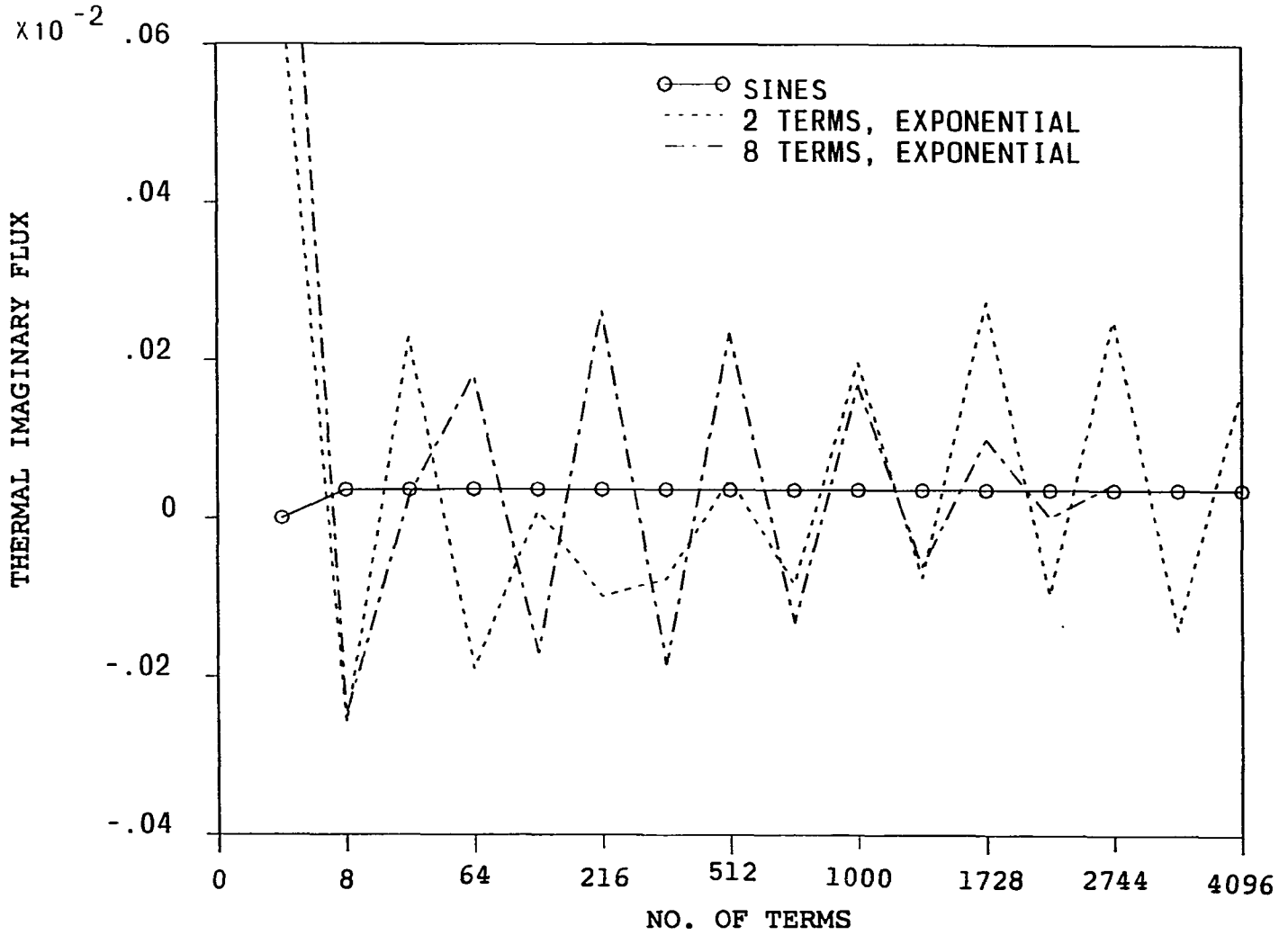

Figure 5.5. Thermal imaginary flux at mesh point (35,40,45) with source located at (50,50,50) and frequency of 10 rad/s calculated using all three analytical solution formulations

VI. THE NODAL SOLUTION

A. Introduction

The nodal diffusion theory, computer code used in this analysis was developed by A. F. Rohach (32, 33, 34). It solves the multigroup diffusion equations by using a polynomial nodal model. The group fluxes were expanded as trial functions in fourth order Legendre polynomials about the center point of each node. A function of the difference between the derivative terms and the rest of the terms for the trial fluxes in the multigroup diffusion equation was developed. The squares of the residual function were minimized with respect to the Legendre polynomial coefficients over each node. Using interface conditions for each node in addition to the minimization relations, five, fifteen and thirty five nodal relations were obtained for the one-, two- and three-dimensional problems respectively.

Leakage currents between nodes were considered by expanding the flux at a small distance from the node interface in a Taylor series in terms of the node interface fluxes and applying continuity relations of neutron fluxes and currents between nodes. Finally, the nodal relations were used to calculate Legendre polynomial coefficients.

B. Development of the 3-D Model Equations

The following is the development procedure of the three-dimensional nodal model equations by Rohach (34).

The three-dimensional region is shown in Figure 6.1. Each node (i,j,k) is represented with its own coordinate system centered at the node center. The three-dimensional multigroup diffusion equation with constant neutronic parameters is

$$D_g \left(\frac{\partial^2 \phi_g(x,y,z)}{\partial x^2} + \frac{\partial^2 \phi_g(x,y,z)}{\partial y^2} + \frac{\partial^2 \phi_g(x,y,z)}{\partial z^2} \right)$$

$$- \Sigma_t^g \phi_g(x,y,z) + \sum_{h=1}^{G} \left(\Sigma_s^{hg} + \frac{\chi^g}{\lambda} \Sigma_f^h \right) \phi_h(x,y,z) = 0 \qquad (6.1)$$

for $g = 1, 2, \ldots G$

where

$$\Sigma_t^g = \Sigma_a^g + \Sigma_s^g = \Sigma_a^g + \sum_{h=1}^{G} \Sigma_s^{hg} \qquad (6.2)$$

Rewrite the equation in the form

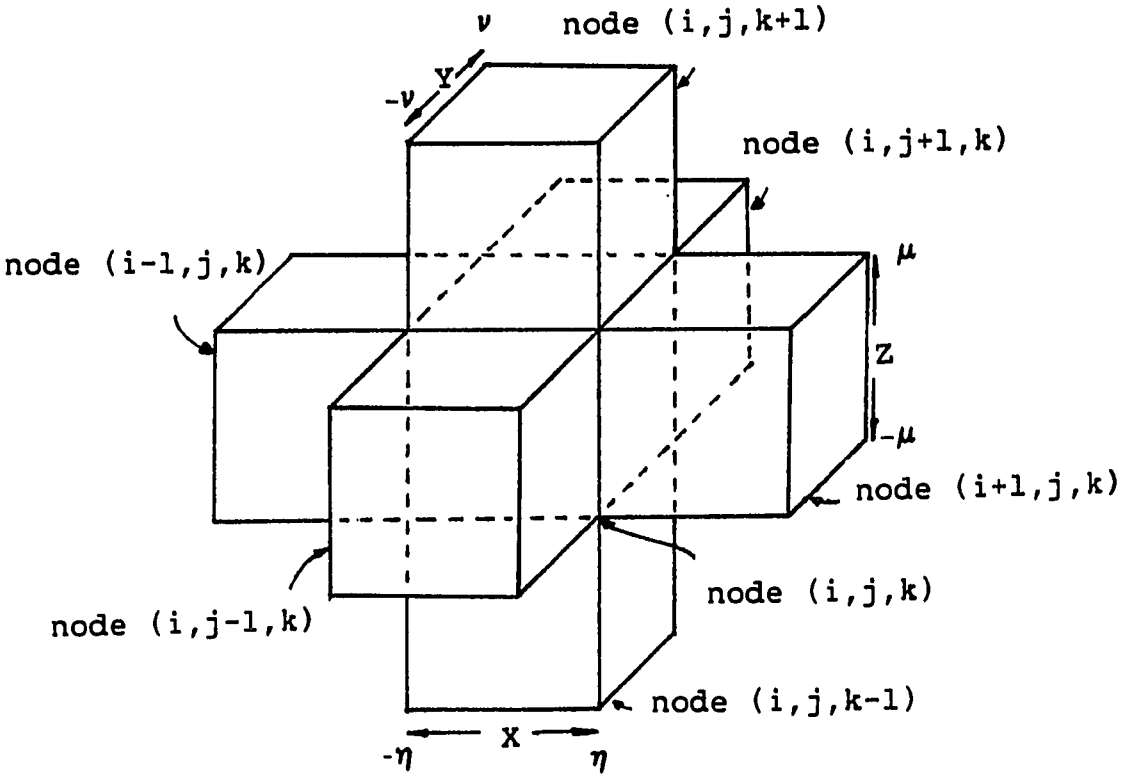

Figure 6.1. The three-dimensional nodal geometry

$$\frac{\partial^2 \phi_g(x,y,z)}{\partial x^2} + \frac{\partial^2 \phi_g(x,y,z)}{\partial y^2} + \frac{\partial^2 \phi_g(x,y,z)}{\partial z^2}$$

$$+ \sum_{h=1}^{G} a_{gh}\ \phi_h(x,y,z) = 0 \qquad (6.3)$$

where

$$a_{gh} = \frac{1}{D_g} \left(\frac{\chi^g}{\lambda} \Sigma_f^h + \Sigma_s^{gh} - \delta_{gh} \Sigma_t^g \right) \qquad (6.4)$$

δ_{gh} = Kronecker delta

The flux will be expanded in the nodal coordinate system in Legendre polynomials in the dimensionless variables u, v, and w. In particular, a fourth order expansion will be used. Therefore

$$\psi^g(u,v,w) = \sum_{l=0}^{4} \sum_{m=0}^{4-l} \sum_{n=0}^{4-l-m} a_{lmn}^g\ P_l(u)\ P_m(v)\ P_n(w) \qquad (6.5)$$

where

$$u = \frac{x}{\eta}\ ;\ v = \frac{y}{\nu}\ ;\ w = \frac{z}{\mu} \qquad (6.6)$$

One can calculate the second derivative of equation (6.5) as

$$\left(\frac{\partial^2}{\partial x^2} + \frac{\partial^2}{\partial y^2} + \frac{\partial^2}{\partial z^2}\right) \psi^g(u,v,w)$$

$$= \sum_{l=0}^{2} \sum_{m=0}^{2-l} \sum_{n=0}^{2-l-m} \tilde{a}^g_{lmn} P_l(u) P_m(v) P_n(w) \qquad (6.7)$$

where $\tilde{a}^g_{lmn}$ are functions of a^g_{lmn}.

Now substitute the polynomial expansion (equation 6.5) into equation (6.3). Since the approximate solutions will not exactly satisfy equation (6.3), we define the residual function

$$f_g(u,v,w) = \sum_{l=0}^{2} \sum_{m=0}^{2-l} \sum_{n=0}^{2-l-m} \tilde{a}^g_{lmn} P_l(u) P_m(v) P_n(w)$$

$$+ \sum_{l=0}^{4} \sum_{m=0}^{4-l} \sum_{n=0}^{4-l-m} c^g_{lmn} P_l(u) P_m(v) P_n(w)$$

$$= f_{1g}(u,v,w) + f_{2g}(u,v,w) \qquad (6.8)$$

where

$$c^g_{lmn} = \sum_{h=1}^{G} \alpha_{gh} a^h_{lmn} \qquad (6.9)$$

We want to minimize the least squares of the function $f_g(u,v,w)$ over the nodal interval with respect to the polynomial coefficients:

$$\frac{\partial}{\partial a_{lmn}} \int_{-1}^{+1} du \int_{-1}^{+1} dv \int_{-1}^{+1} dw \; f_g^2(u,v,w) = 0 \; ; \; l+m+n \leq 4 \qquad (6.10)$$

However when the minimization process is performed, it will be assumed that $f_{2g}(u,v,w)$ is independent of the coefficients. In the process, the minimization is the difference between the derivative terms and the rest of the terms in equation (6.3). Therefore the minimization will be the least-squares difference between a second order polynomial and a fourth order polynomial. The resulting relations can be written as

$$\tilde{a}^g_{lmn} + c^g_{lmn} = 0 \; ; \; l+m+n \leq 2 \; ; \text{ all groups } g \qquad (6.11)$$

The properties of orthogonality of the Legendre polynomials were used to get these relations. Therefore we have eight equations for each group to evaluate 35 polynomial coefficients. The continuity conditions at the interfaces will be used to get the remaining necessary conditions. Interface-matching conditions can be determined for the boundaries of the node (Figure 6.2). One would require continuity of the function on the boundary. Of course, with a finite order of polynomials this requirement

can not be met at every point on the boundary. Therefore we only require continuity of the average function over the eight regions shown in Figure 6.2. From these we can define 24 average fluxes at the appropriate boundaries. The average fluxes in the x-direction can be defined as

$$\psi^g_{\mp++} \equiv \int_0^1 dv \int_0^1 dw\ \psi^g(u,v,w) \Big|_{u=\mp 1}$$

$$= \psi^g_{100} \mp \psi^g_{200} + \psi^g_{300} + \psi^g_{400} \mp \psi^g_{500} \mp \psi^g_{600} + \psi^g_{700} \mp \psi^g_{800}$$

$$\psi^g_{\mp-+} \equiv \int_{-1}^0 dv \int_0^1 dw\ \psi^g(u,v,w) \Big|_{u=\mp 1}$$

$$= \psi^g_{100} \mp \psi^g_{200} - \psi^g_{300} + \psi^g_{400} \mp \psi^g_{500} \mp \psi^g_{600} - \psi^g_{700} \mp \psi^g_{800}$$

$$\psi^g_{\mp+-} \equiv \int_0^1 dv \int_{-1}^0 dw\ \psi^g(u,v,w) \Big|_{u=\mp 1} \qquad (6.12)$$

$$= \psi^g_{100} \mp \psi^g_{200} + \psi^g_{300} - \psi^g_{400} \mp \psi^g_{500} \mp \psi^g_{600} - \psi^g_{700} \mp \psi^g_{800}$$

$$\psi^g_{\mp--} \equiv \int_{-1}^0 dv \int_{-1}^0 dw\ \psi^g(u,v,w) \Big|_{u=\mp 1}$$

$$= \psi^g_{100} \mp \psi^g_{200} - \psi^g_{300} - \psi^g_{400} \mp \psi^g_{500} \mp \psi^g_{600} + \psi^g_{700} \mp \psi^g_{800}$$

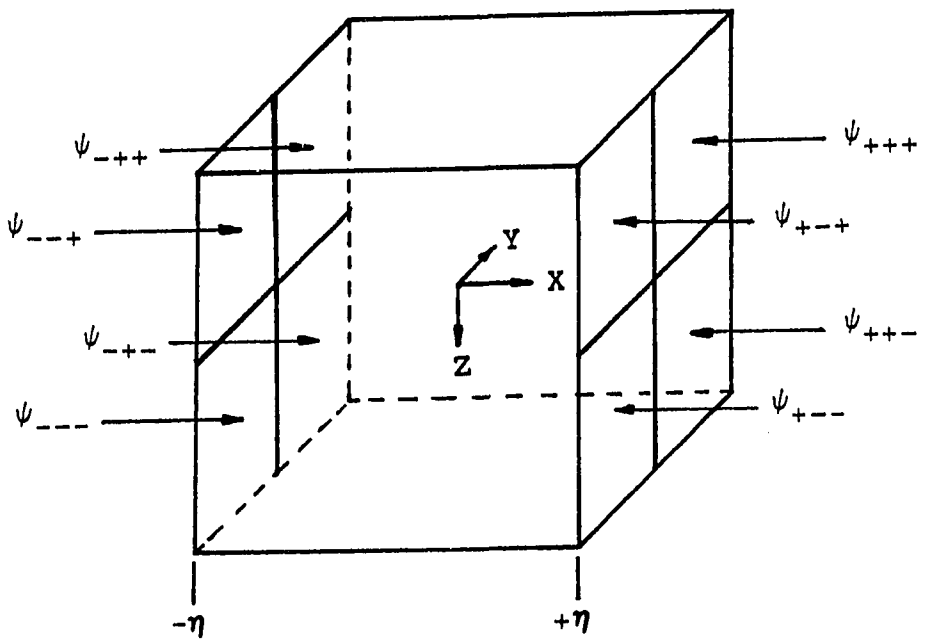

Figure 6.2. The average node flux at $x = \mp\eta$

where

$$\psi^g_{100} = a^g_{000} + a^g_{200} + a^g_{400}$$

$$\psi^g_{200} = a^g_{100} + a^g_{300}$$

$$\psi^g_{300} = \frac{1}{2}\left(a^g_{010} + a^g_{210} - \frac{a^g_{030}}{4}\right)$$

$$\psi^g_{400} = \frac{1}{2}\left(a^g_{001} + a^g_{201} - \frac{a^g_{003}}{4}\right)$$

$$\psi^g_{500} = \frac{1}{2}\left(a^g_{110} + a^g_{310} - \frac{a^g_{130}}{4}\right) \qquad (6.13)$$

$$\psi^g_{600} = \frac{1}{2}\left(a^g_{101} + a^g_{301} - \frac{a^g_{103}}{4}\right)$$

$$\psi^g_{700} = \frac{1}{4}\left(a^g_{011} + a^g_{211} - \frac{a^g_{031} + a^g_{013}}{4}\right)$$

$$\psi^g_{800} = \frac{1}{4}\, a^g_{111}$$

Similar integrals can be defined for the y-direction and the z-direction. One can use relations 6.13 to also determine the following relations:

$$\psi^g_{100} = \frac{1}{4}(\psi^g_{+++}+\psi^g_{+-+}+\psi^g_{++-}+\psi^g_{+--}+\psi^g_{-++}+\psi^g_{--+}+\psi^g_{-+-}+\psi^g_{---})$$

$$\psi^g_{200} = \frac{1}{4}(\psi^g_{+++}+\psi^g_{+-+}+\psi^g_{++-}+\psi^g_{+--}-\psi^g_{-++}-\psi^g_{--+}-\psi^g_{-+-}-\psi^g_{---})$$

$$\psi^g_{300} = \frac{1}{4}(\psi^g_{+++}-\psi^g_{+-+}+\psi^g_{++-}-\psi^g_{+--}+\psi^g_{-++}-\psi^g_{--+}+\psi^g_{-+-}-\psi^g_{---})$$

$$\psi^g_{400} = \frac{1}{4}(\psi^g_{+++}+\psi^g_{+-+}-\psi^g_{++-}-\psi^g_{+--}+\psi^g_{-++}+\psi^g_{--+}-\psi^g_{-+-}-\psi^g_{---})$$

$$\psi^g_{500} = \frac{1}{4}(\psi^g_{+++}-\psi^g_{+-+}+\psi^g_{++-}-\psi^g_{+--}-\psi^g_{-++}+\psi^g_{--+}-\psi^g_{-+-}+\psi^g_{---})$$

$$\psi^g_{600} = \frac{1}{4}(\psi^g_{+++}+\psi^g_{+-+}-\psi^g_{++-}-\psi^g_{+--}-\psi^g_{-++}-\psi^g_{--+}+\psi^g_{-+-}+\psi^g_{---})$$

$$\psi^g_{700} = \frac{1}{4}(\psi^g_{+++}-\psi^g_{+-+}-\psi^g_{++-}+\psi^g_{+--}+\psi^g_{-++}-\psi^g_{--+}-\psi^g_{-+-}+\psi^g_{---})$$

$$\psi^g_{800} = \frac{1}{4}(\psi^g_{+++}-\psi^g_{+-+}-\psi^g_{++-}+\psi^g_{+--}-\psi^g_{-++}+\psi^g_{--+}+\psi^g_{-+-}-\psi^g_{---})$$

(6.14)

Sixteen more relations can be developed for the y and z-directions by interchanging the subscripts.

Now one can solve for the following coefficients

$$a^g_{300} = \frac{\frac{6}{a_{gg}\nu^2}\psi^g_{040} + \frac{6}{a_{gg}\mu^2}\psi^g_{003}\left(1 - \frac{3}{a_{gg}\nu^2} - \frac{3}{a_{gg}\mu^2}\right)\psi^g_{200} + \frac{\tilde{c}^g_{100}}{a_{gg}}}{1 - \frac{15}{a_{gg}\eta^2} - \frac{15}{4a_{gg}\nu^2} - \frac{15}{4a_{gg}\mu^2}}$$

$$a^g_{100} = \psi^g_{200} - a^g_{300}$$

$$a^g_{120} = 2\psi^g_{040} - a^g_{100} + \frac{1}{4}a^g_{300}$$

$$a^g_{102} = 2\psi^g_{003} - a^g_{100} + \frac{1}{4}a^g_{300}$$

$$a^g_{030} = \frac{\frac{6}{a_{gg}\mu^2}\psi^g_{004} + \frac{6}{a_{gg}\eta^2}\psi^g_{300}\left(1 - \frac{3}{a_{gg}\mu^2} - \frac{3}{a_{gg}\eta^2}\right)\psi^g_{020} + \frac{\tilde{c}^g_{010}}{a_{gg}}}{1 - \frac{15}{a_{gg}\nu^2} - \frac{15}{4a_{gg}\mu^2} - \frac{15}{4a_{gg}\eta^2}}$$

$$a^g_{010} = \psi^g_{020} - a^g_{030}$$

$$a^g_{012} = 2\psi^g_{004} - a^g_{010} + \frac{1}{4}a^g_{030}$$

$$a^g_{210} = 2\psi^g_{300} - a^g_{010} + \frac{1}{4}a^g_{030}$$

$$a^g_{003} = \frac{\frac{6}{a_{gg}\eta^2}\psi^g_{400} + \frac{6}{a_{gg}\nu^2}\psi^g_{030}\left(1 - \frac{3}{a_{gg}\eta^2} - \frac{3}{a_{gg}\nu^2}\right)\psi^g_{002} + \frac{\tilde{c}^g_{001}}{a_{gg}}}{1 - \frac{15}{a_{gg}\mu^2} - \frac{15}{4a_{gg}\eta^2} - \frac{15}{4a_{gg}\nu^2}}$$

$$a^g_{001} = a^g_{002} - a^g_{003}$$

$$a^g_{201} = 2\psi^g_{400} - a^g_{001} + \frac{1}{4}a^g_{003}$$

$$a^g_{021} = 2\psi^g_{030} - a^g_{001} + \frac{1}{4}a^g_{003}$$

$$a^g_{130} = \frac{2\left(\frac{12}{a_{gg}\eta^2} + \frac{1}{5}\right)\psi^g_{500} + 2\left(\frac{4}{5} - \frac{12}{a_{gg}\nu^2} - \frac{3}{a_{gg}\mu^2}\right)\psi^g_{060} + \psi^g_{007} + \frac{\tilde{c}^g_{110}}{a_{gg}}}{\frac{3}{4}\left(1 - \frac{20}{a_{gg}\eta^2} - \frac{20}{a_{gg}\nu^2} - \frac{20}{4a_{gg}\mu^2}\right)}$$

$$a^g_{310} = \frac{2\left(\frac{12}{a_{gg}\nu^2} + \frac{1}{5}\right)\psi^g_{060} + 2\left(\frac{4}{5} - \frac{12}{a_{gg}\eta^2} - \frac{3}{a_{gg}\mu^2}\right)\psi^g_{500} + \psi^g_{007} + \frac{\tilde{c}^g_{110}}{a_{gg}}}{\frac{3}{4}\left(1 - \frac{20}{a_{gg}\nu^2} - \frac{20}{a_{gg}\eta^2} - \frac{20}{4a_{gg}\mu^2}\right)}$$

$$a^g_{110} = \psi^g_{500} + \psi^g_{060} - \frac{3}{8}\left(a^g_{310} + a^g_{130}\right)$$

$$a^g_{112} = 4\psi^g_{007} - \psi^g_{500} - \psi^g_{060} + \frac{5}{8}\left(a^g_{310} + a^g_{130}\right)$$

$$a^g_{013} = \frac{2\left(\frac{12}{a_{gg}\nu^2}+\frac{1}{5}\right)\psi^g_{050}+2\left(\frac{4}{5}-\frac{12}{a_{gg}\mu^2}-\frac{3}{a_{gg}\eta^2}\right)\psi^g_{006}+\psi^g_{700}+\frac{\tilde{c}^g_{011}}{a_{gg}}}{\frac{3}{4}\left(1-\frac{20}{a_{gg}\nu^2}-\frac{20}{a_{gg}\mu^2}-\frac{20}{4a_{gg}\eta^2}\right)}$$

$$a^g_{031} = \frac{2\left(\frac{12}{a_{gg}\mu^2}+\frac{1}{5}\right)\psi^g_{006}+2\left(\frac{4}{5}-\frac{12}{a_{gg}\nu^2}-\frac{3}{a_{gg}\eta^2}\right)\psi^g_{050}+\psi^g_{700}+\frac{\tilde{c}^g_{011}}{a_{gg}}}{\frac{3}{4}\left(1-\frac{20}{a_{gg}\mu^2}-\frac{20}{a_{gg}\nu^2}-\frac{20}{4a_{gg}\eta^2}\right)}$$

$$a^g_{011} = \psi^g_{050} + \psi^g_{006} - \frac{3}{8}\left(a^g_{031} + a^g_{013}\right)$$

$$a^g_{211} = 4\psi^g_{700} - \psi^g_{050} - \psi^g_{006} + \frac{5}{8}\left(a^g_{031} + a^g_{013}\right)$$

$$a^g_{301} = \frac{2\left(\frac{12}{a_{gg}\mu^2}+\frac{1}{5}\right)\psi^g_{005}+2\left(\frac{4}{5}-\frac{12}{a_{gg}\eta^2}-\frac{3}{a_{gg}\nu^2}\right)\psi^g_{600}+\psi^g_{070}+\frac{\tilde{c}^g_{101}}{a_{gg}}}{\frac{3}{4}\left(1-\frac{20}{a_{gg}\mu^2}-\frac{20}{a_{gg}\eta^2}-\frac{20}{4a_{gg}\nu^2}\right)}$$

$$a^g_{103} = \frac{2\left(\frac{12}{a_{gg}\eta^2}+\frac{1}{5}\right)\psi^g_{600}+2\left(\frac{4}{5}-\frac{12}{a_{gg}\mu^2}-\frac{3}{a_{gg}\nu^2}\right)\psi^g_{005}+\psi^g_{070}+\frac{\tilde{c}^g_{101}}{a_{gg}}}{\frac{3}{4}\left(1-\frac{20}{a_{gg}\eta^2}-\frac{20}{a_{gg}\mu^2}-\frac{20}{4a_{gg}\nu^2}\right)}$$

$$a^g_{101} = \psi^g_{005} + \psi^g_{600} - \frac{3}{8}(a^g_{103} + a^g_{301})$$

$$a^g_{121} = 4\psi^g_{070} - \psi^g_{005} - \psi^g_{600} + \frac{5}{8}(a^g_{103} + a^g_{301})$$

(6.15)

This leaves seven relations to evaluate ten coefficients. In this analysis the coefficients a^g_{220}, a^g_{022}, and a^g_{202} will not be used. Therefore, the remaining seven equations can be solved for the remaining coefficients. By substitution one can reduce the seven-equation system to a three-equation system which can be solved using Gaussian elimination. Therefore one has

$$a^g_{000} = -\frac{e^g_1 - \frac{d^g_{12}}{d^g_{22}}e^g_2 - \frac{d^g_{13}}{d^g_{33}}e^g_3 - \frac{d^g_{14}}{d^g_{44}}e^g_4}{d^g_{11} - \frac{d^g_{12}}{d^g_{22}}d^g_{21} - \frac{d^g_{13}}{d^g_{33}}d^g_{31} - \frac{d^g_{14}}{d^g_{44}}d^g_{41}}$$

$$a^g_{400} = -\frac{e^g_2 + d^g_{21}a^g_{000}}{d^g_{22}} \qquad (6.16)$$

$$a^g_{040} = -\frac{e^g_3 + d^g_{21}a^g_{000}}{d^g_{33}}$$

$$a^g_{004} = -\frac{e^g_4 + d^g_{41}a^g_{000}}{d^g_{44}}$$

$$a^g_{200} = \psi^g_{100} - a^g_{000} - \psi^g_{400}$$

$$a^g_{020} = \psi^g_{010} - a^g_{000} - a^g_{040}$$

$$a^g_{002} = \psi^g_{001} - a^g_{000} - a^g_{004}$$

where

$$d^g_{11} = 1 - \frac{3}{a_{gg}\eta^2} - \frac{3}{a_{gg}\nu^2} - \frac{3}{a_{gg}\mu^2}$$

$$d^g_{12} = \frac{7}{a_{gg}\eta^2} \; ; \quad d^g_{12} = \frac{7}{a_{gg}\nu^2} \; ; \quad d^g_{14} = \frac{7}{a_{gg}\mu^2}$$

$$d^g_{21} = \frac{3}{a_{gg}\mu^2} - 1 \; ; \quad d^g_{22} = \frac{35}{a_{gg}\eta^2} - 1$$

$$d^g_{31} = \frac{3}{a_{gg}\eta^2} - 1 \; ; \quad d^g_{33} = \frac{35}{a_{gg}\nu^2} - 1$$

$$d^g_{41} = \frac{3}{a_{gg}\nu^2} - 1 \; ; \quad d^g_{44} = \frac{35}{a_{gg}\mu^2} - 1 \qquad (6.17)$$

$$e^g_1 = \frac{3}{a_{gg}\eta^2}\psi^g_{100} + \frac{3}{a_{gg}\nu^2}\psi^g_{010} + \frac{3}{a_{gg}\mu^2}\psi^g_{001} + \frac{\tilde{c}^g_{000}}{a_{gg}}$$

$$e^g_2 = \frac{3}{a_{gg}\mu^2}\left(\frac{\psi^g_{101}}{4} - \psi^g_{001}\right) + \left(1 - \frac{3}{a_{gg}\mu^2}\right)\psi^g_{100} + \frac{\tilde{c}^g_{200}}{a_{gg}}$$

$$e_3^g = \frac{3}{a_{gg}\eta^2}\left(\frac{\psi_{110}^g}{4}-\psi_{100}^g\right) + \left(1-\frac{3}{a_{gg}\eta^2}\right)\psi_{010}^g + \frac{\tilde{c}_{020}^g}{a_{gg}}$$

$$e_4^g = \frac{3}{a_{gg}\nu^2}\left(\frac{\psi_{011}^g}{4}-\psi_{010}^g\right) + \left(1-\frac{3}{a_{gg}\nu^2}\right)\psi_{001}^g + \frac{\tilde{c}_{002}^g}{a_{gg}}$$

Now there are 32 nodal relations (24 boundary average fluxes and eight minimization equations) from which to evaluate the polynomial coefficients. One can easily require the nodal average boundary fluxes to be continuous; however relations are needed to connect the leakage currents between nodes.

One can expand the fluxes at a distance θ from the node interfaces in a Taylor series in terms of the node interface fluxes. One relation at interface $x = \eta_i$ in node (i,j,k) is

$$\psi_{ijk}^g(1-\theta,v,w) = \sum_{n=0}^{\infty}\frac{(-\theta)^n}{n}\frac{\partial^n}{\partial u^n}\psi_{ijk}^g(u,v,w)\Big|_{u=1} \qquad (6.18)$$

which must hold at every value of y and z on the $x = \eta_i$ interface. A similar relation can be developed on the other side of the interface in node (i+1,j,k).

$$\psi_{i+1,jk}^g(\theta-1,v,w) = \sum_{n=0}^{\infty}\frac{\theta^n}{n}\frac{\partial^n}{\partial x^n}\psi_{i+1,jk}^g(u,v,w)\Big|_{u=-1} \qquad (6.19)$$

If one requires both continuity of flux and current then at

one interface

$$\psi^g(1,v,w)\Big|_{\text{node}(i,j,k)} = \psi^g(-1,v,w)\Big|_{\text{node}(i+1,j,k)} \tag{6.20}$$

$$-D_g\psi_x^g(1,v,w)\Big|_{\text{node}(i,j,k)} = -D_g\psi_x^g(-1,v,w)\Big|_{\text{node}(i+1,j,k)} \tag{6.21}$$

However since the expansions are only in a finite number of polynomials, these relations can not be satisfied at every interface point. Therefore one only requires continuity of the average relation over a quarter of the node surface

$$\int_0^{+1} dv \int_0^{+1} dw\ \psi^g(1,v,w)\ \Big|_{\text{node}(i,j,k)}$$

$$= \int_0^{+1} dv \int_0^{+1} dw\ \psi^g(-1,v,w)\ \Big|_{\text{node}(i+1,j,k)} \tag{6.22}$$

$$\int_0^{+1} dv \int_0^{+1} dw\ -D_g\psi_x^g(1,v,w)\ \Big|_{\text{node}(i,j,k)}$$

$$= \int_0^{+1} dv \int_0^{+1} dw\ -D_g\psi_x^g(-1,v,w)\ \Big|_{\text{node}(i+1,j,k)} \tag{6.23}$$

If equations (6.22) and (6.23) are integrated over the node surface for the function from equation (6.3) and if the

higher derivatives are evaluated for the coefficients, then the average flux on the surfaces can be estimated from

$$\psi^g_{+\mp+ijk}\left(\frac{D^g_{ijk}}{\eta_i}+\frac{D^g_{i+1,jk}}{\eta_{i+1}}\right)$$

$$=\sum_{n=0}^{4}\left[1-\frac{n}{2}(n+1)\theta\right]\left(\frac{D^g_{ijk}}{\eta_i}\tilde{a}^g_{n\ ijk}+(-1)^n\frac{D^g_{i+1,jk}}{\eta_{i+1}}\tilde{a}^g_{n\ ijk}\right) \tag{6.24}$$

where

$$\tilde{a}^g_0 = a^g_{000}+\frac{1}{2}(\mp a^g_{010}+a^g_{001})\mp\frac{1}{4}a^g_{111}$$

$$-\frac{1}{8}(\mp a^g_{030}+a^g_{003})-\frac{1}{16}(\mp a^g_{031}\mp a^g_{013}) \tag{6.25}$$

$$\tilde{a}^g_1 = \mp a^g_{100}+\frac{1}{2}(\mp a^g_{110}+a^g_{101})\mp\frac{1}{4}a^g_{111}+\frac{1}{8}(\mp a^g_{130}+a^g_{103})$$

$$\tilde{a}^g_2 = a^g_{200}+\frac{1}{2}(\mp a^g_{210}+a^g_{201})\mp\frac{1}{4}a^g_{211}$$

$$\tilde{a}^g_3 = a^g_{300}+\frac{1}{2}(\mp a^g_{310}+a^g_{301})$$

$$\tilde{a}^g_4 = a^g_{400}$$

Similar relations can be derived for the other half of the surface. Again similar relations can be developed for the other five interface surfaces. Therefore one can evaluate the flux coefficients from the nodal average interface values and the minimization conditions. The interface values, in turn, can be evaluated from the coefficients and an iterative solution can be established.

The core eigenvalue can be determined from the neutron balance over all nodes and the following expression results :

$$\lambda = \frac{\sum_{i=1}^{I}\sum_{j=1}^{J}\sum_{k=1}^{K}\eta_i\nu_j\mu_k\sum_{g=1}^{G}\nu\Sigma_{fijk}^{g}a_{0ijk}^{g}}{\sum_{i=1}^{I}\sum_{j=1}^{J}\sum_{k=1}^{K}\sum_{g=1}^{G}\left(\eta_i\nu_j\mu_k\Sigma_{aijk}^{g}a_{0ijk}^{g}\right.} \tag{6.26}$$

$$-D_{ijk}^{g}\left(\frac{\nu_j\mu_k}{\eta_i}(3a_{200}^{g}+10a_{400}^{g})_{ijk}+\frac{\eta_i\mu_k}{\nu_j}(3a_{020}^{g}\right.$$

$$\left.\left.+10a_{040}^{g})_{ijk}+\frac{\mu_k\eta_i}{\mu_k}(3a_{002}^{g}+10a_{004}^{g})_{ijk}\right)\right)$$

C. Generating Input Data

Since the nodal code was originally developed to handle multigroup diffusion problems, simple changes were required

to adjust the program to accept negative fluxes and to assure convergence, particularly when the difference between the group fluxes could be several orders of magnitudes. Moreover, the four equations of the two-group frequency-dependent problem must be cast in a form similar to the four neutron energy groups equations to be accepted by the code. Therefore, a program was written to generate the four-group equivalent parameters from the two-group data presented in Table 4.1. The input generating program is listed in Appendix A.

D. Source Representation

Although the local perturbation in the thermal absorption cross section was considered to be located at the common corner point of eight nodes, it was represented as a set of plane sources given as interface conditions on one-fourth of the eight node boundary surfaces as shown in Figure 6.3. Therefore, the point source was actually approximated by three intersecting surfaces extending from the center line of the interface surfaces of these eight nodes. This approximation is correct only if these eight nodes are infinitly small. Since this research deals only with source problems, the eigenvalue of equation (6.26) will not be used.

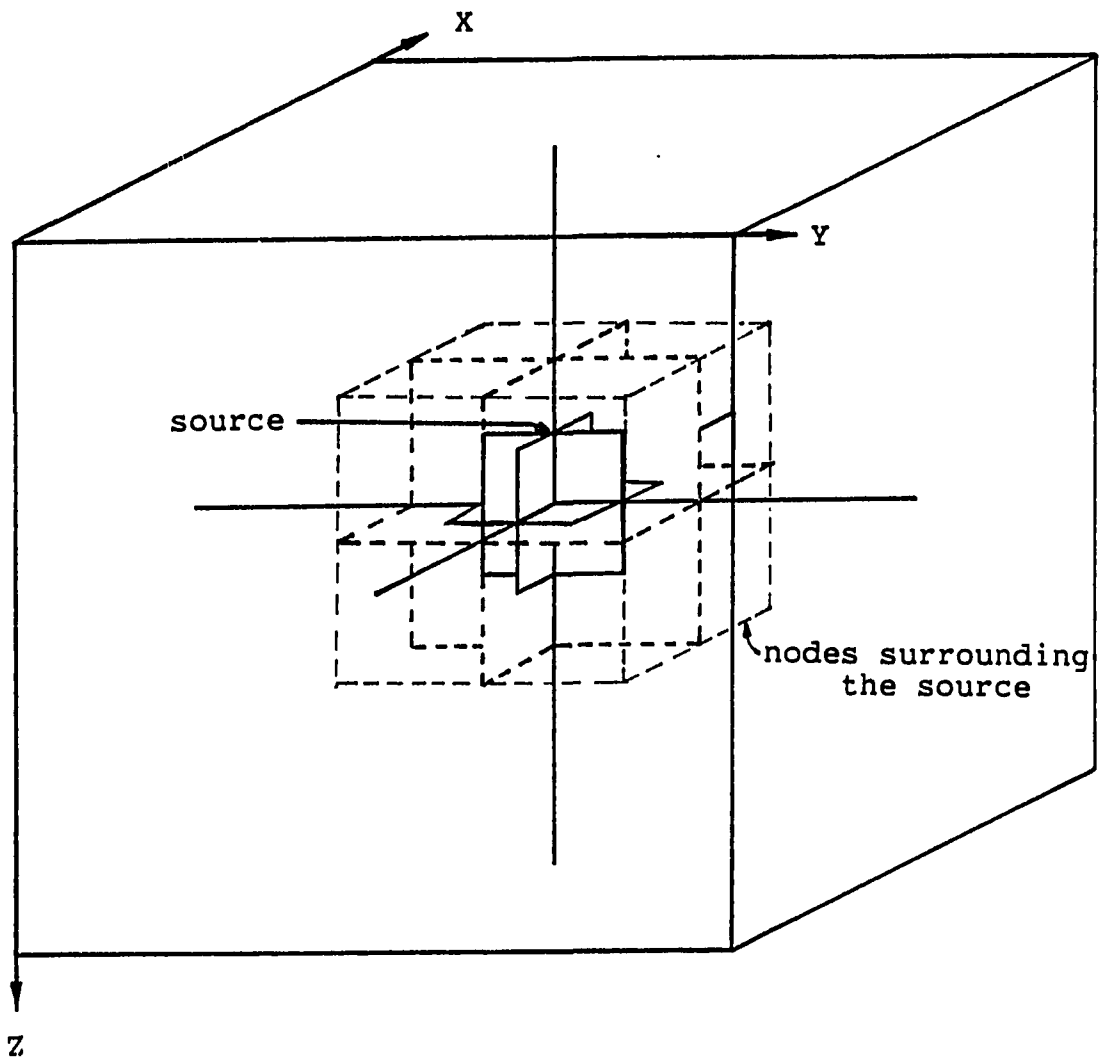

Figure 6.3. The point source representation in the nodal model

VII. RESULTS AND ANALYSIS

As pointed out in the previous chapters, the aim of this research was to develop a nodal solution for the frequency dependent diffusion equations. The task was approached by developing the mathematical equations that represent the frequency dependent problem, modifying a nodal computer program that was originally developed to solve the static multigroup diffusion equations, and testing the nodal model and its validity by comparing its results with results obtained from an analytical solution model. The analytical model was developed and applied using the same restrictions and conditions imposed on the nodal model.

A. The Nodal Code Results

The nodal solution model was tested over the simple cubic geometry shown in Figure 4.1. The cube was 100 cm on a side and material properties were adjusted such that the system was originally critical. The negative source with a strength of 48 neutrons/s (representing $-\Delta\Sigma_a\phi_0$) was located at the center of the cube. As pointed out, the source has the shape of three intersecting planes as shown in Figure 6.1. Applying the nodal computer code to the system yielded the coefficients of the Legendre polynomials. Since the frequency dependent fluxes were expanded in the Legendre polynomials, these coefficients could be used to calculate

flux values at any point in the reactor model. The coefficients were calculated for each neutron energy group inside each node. To show the magnitude and the shape of the fluxes in a three-dimensional model, several planes perpendicular to the z axis were chosen and flux values were calculated at different points on each plane separately. Figures 7.1 through 7.4 show the frequency dependent two-group fluxes on the x-y plane at z=50.0 cm and ω=10 rad/s, where the coefficients were calculated using 216 nodes and node sizes were 20, 15, 15, 15, 15 and 20 cm in each direction. This frequency of 10 rad/s is in the plateau region of the zero power reactor transfer function which extends, as shown in Figure 7.5, from $\omega = \beta/\ell \simeq 527$ rad/s to $\omega = \lambda \simeq 0.1$ rad/s. Since the fluxes are complex quantities, the two-group frequency dependent fluxes yielded four fluxes, a real part and an imaginary part for each group.

The accuracy of the nodal code results depends on the number of nodes used to represent the reactor geometry and source size. Therefore, the nodal code was examined using 8, 64 and 216 nodes over the same reactor model. The execution times for these three cases are shown in Table 7.1. Moreover, the node sizes around the source were reduced and several node sizes were examined. Since the nodal computer code employs an iterative technique,

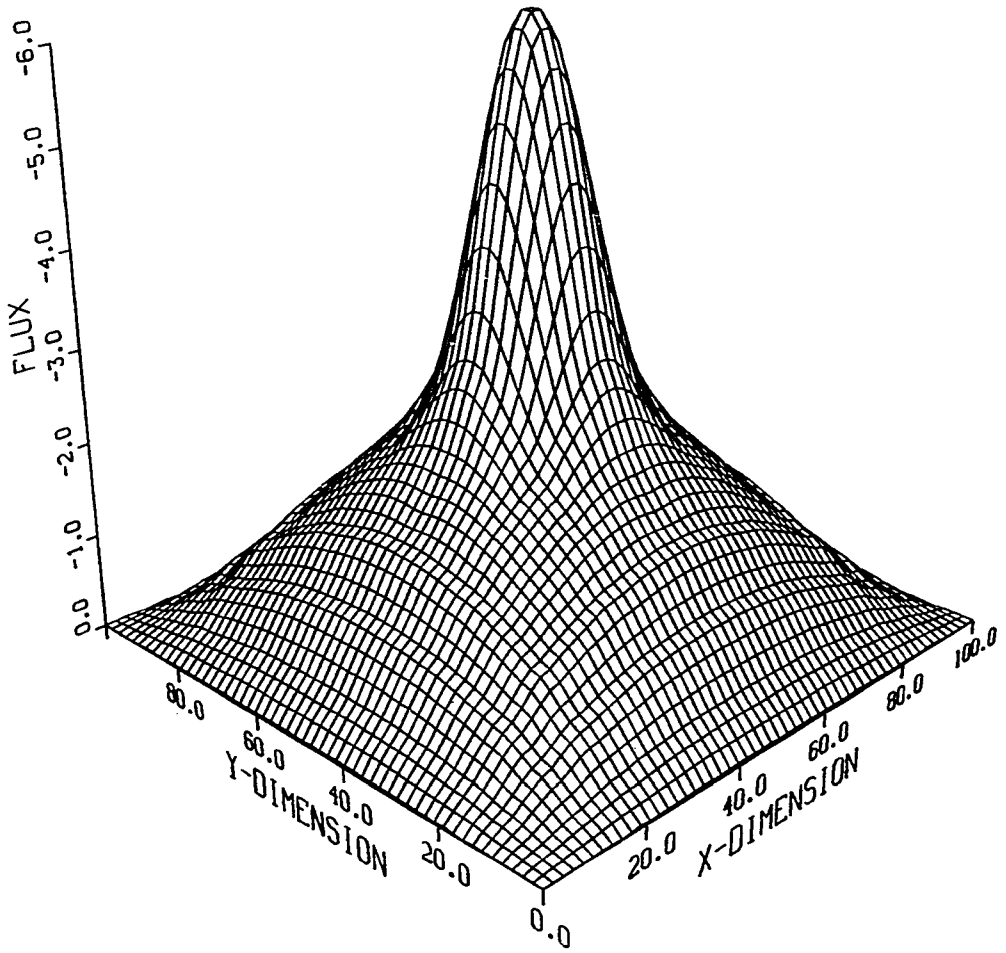

Figure 7.1. The real component of the fast flux in the X-Y plane at Z=50 cm, ω=10 rad/sec, and number of nodes =216

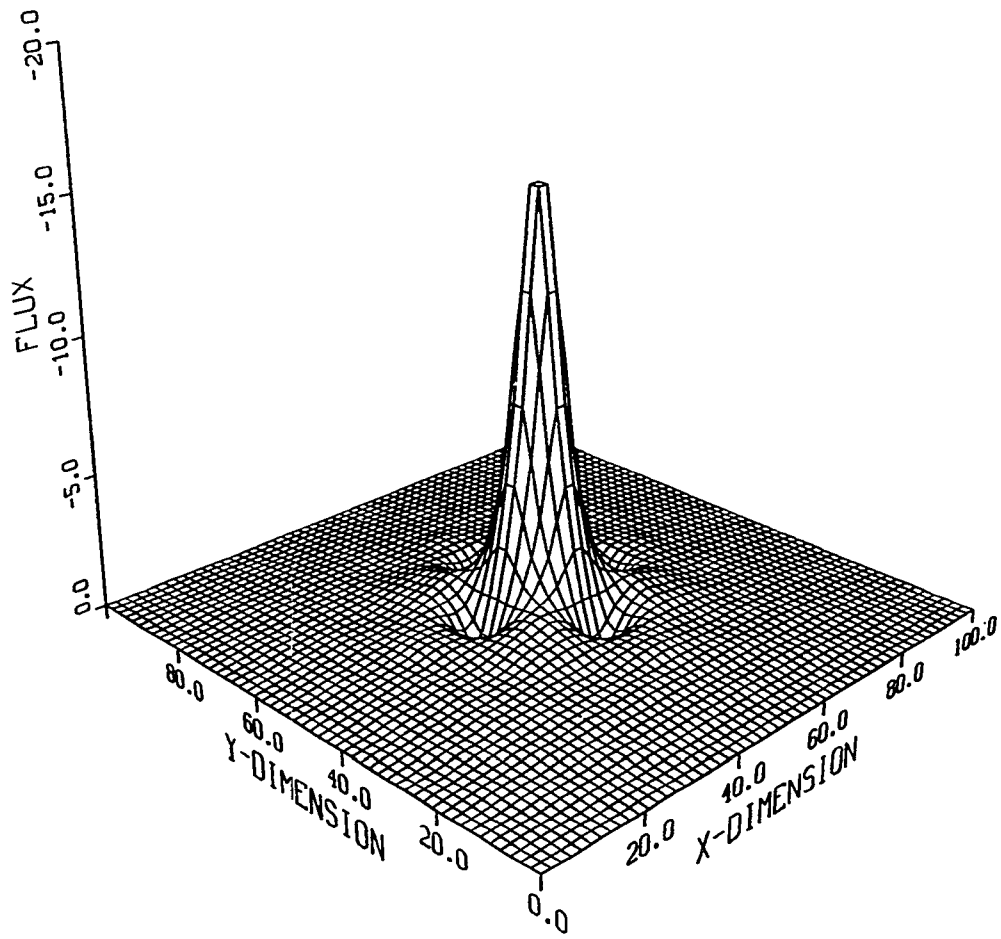

Figure 7.2. The real component of the thermal flux in the X-Y plane at Z=50 cm, ω =10 rad/sec, and number of nodes =216

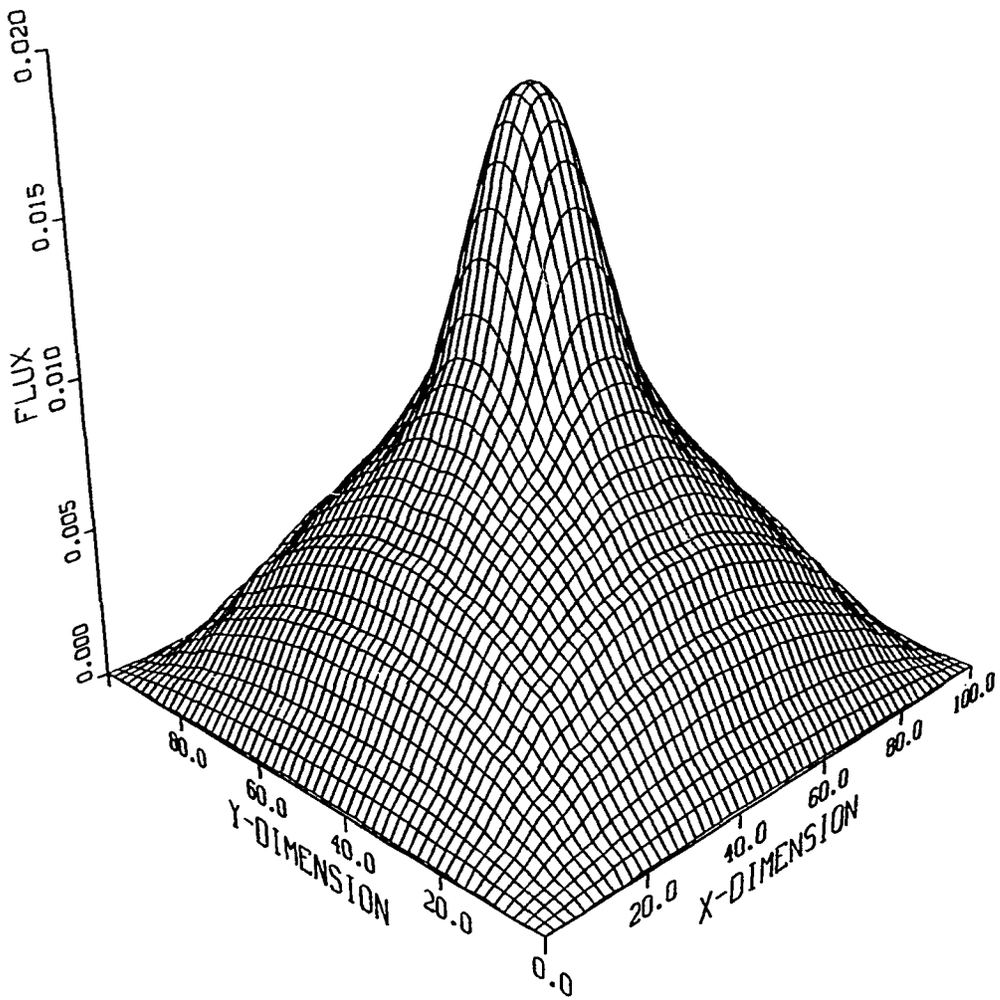

Figure 7.3. The imaginary component of the fast flux in the X-Y plane at Z=50 cm, ω =10 rad/sec, and number of nodes =216

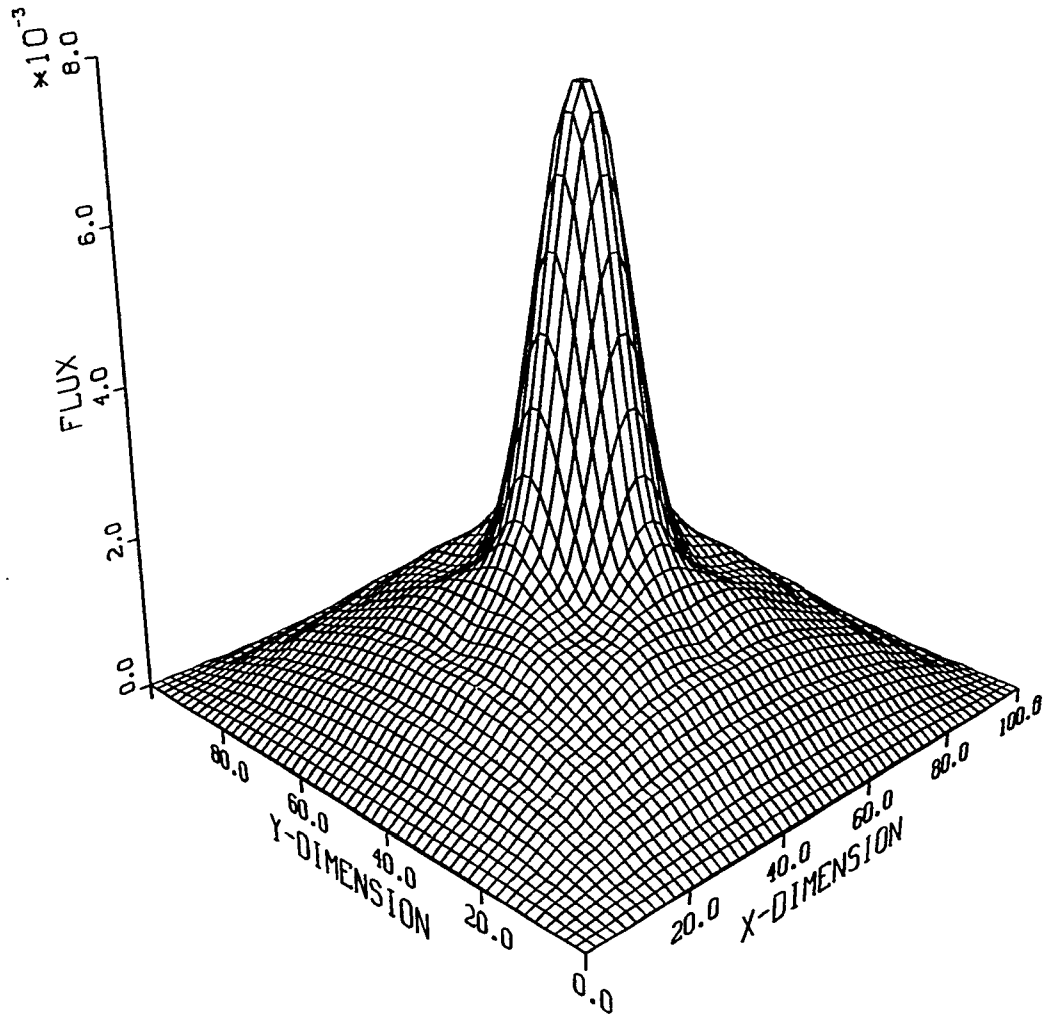

Figure 7.4. The imaginary component of the thermal flux in the X-Y plane at Z=50 cm, ω =10 rad/sec, and number of nodes =216

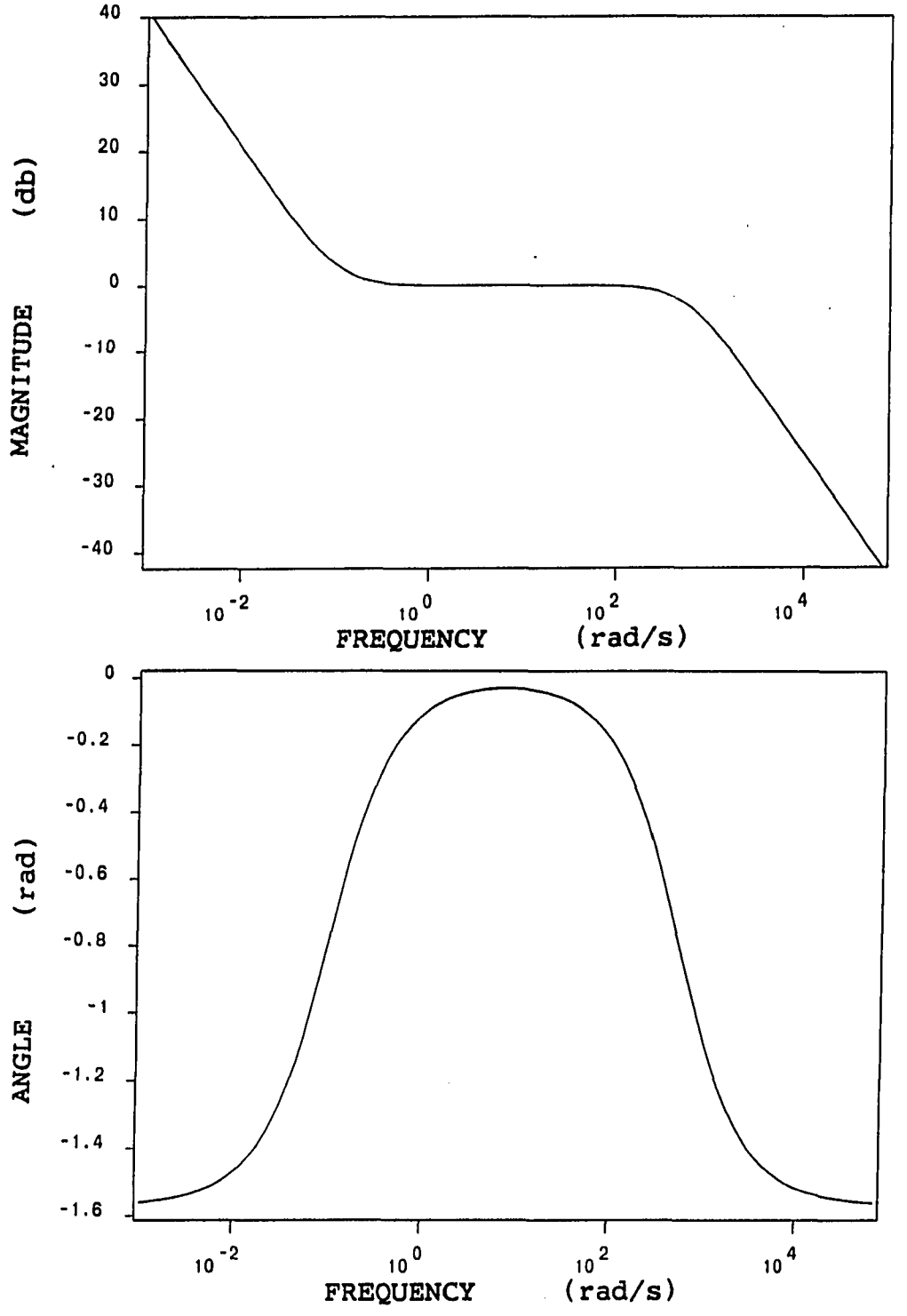

Figure 7.5. Magnitude and phase of the zero power reactor transfer function, (ℓ/β)=1.9E-3 s

Table 7.1 The execution time of the nodal code on the National Advanced System/9160 computer (NAS)

no. of nodes	no of iterations	execution time
8	100	5.50 s
64	100	26.80 s
216	100	86.34 s
216	500	402.38 s

reducing the node size at the source location slowed down convergence to an extent that computation time became a major problem.

Furthermore, the behavior of the nodal code was investigated at frequencies outside the plateau region of the zero power transfer function. The plateau region is bound by $.1 < \omega < 527$ rad/s. Thus, 0.05 rad/s, 200 rad/s and 1000 rad/s frequencies were used.

In all of these cases, the nodal solution model was able to predict the general shape and relative magnitudes of the real and the imaginary fluxes. The magnitude of the frequency dependent fast and thermal fluxes are large at low frequencies, almost constant at frequencies in the plateau region, and small at high frequencies. Furthermore, the

ratio between the real and imaginary parts is very large within the plateau region and gets small at both high and low frequencies.

Depending on the type of perturbation introduced, whether it is a source or a sink of neutrons, the real and imaginary parts of the frequency dependent fluxes have opposite signs. According to the negative neutron source used in this model, the real part of the fluctuation came out to be negative as in Figures 7.1 and 7.2, while the imaginary parts were positive as shown in Figure 7.3 and 7.4.

This general behavior of the solution was verified by the analytical solution and has been reported earlier by several authors (1, 9, 28).

Observing the nodal solution at different levels, perpendicular to the z-axis of the reactor model, shows some irregularities in the flux shape, as in Figure 7.2. These irregularities occur at the node corners because the nodal solution model guarantees only the continuity of neutron flux and current at the interface between nodes but not at node corners. The coefficients a^g_{220}, a^g_{022}, and a^g_{202} could be used to smooth these discontinuities.

B. The Analytical Solution

As a result of investigating the three forms of the analytical solution, the superiority of the triple sine summation form was clear. Therefore, it was applied to verify the results obtained by the nodal code. Both the nodal and the analytical solutions were obtained for the same reactor geometry and using the same reactor material properties. The only difference in applying both methods was in the source geometry. The source was a single point for the analytical solution model while it was described by three intersecting planes for the nodal case. The source view was shown in Figure 6.1.

The analytical solution also showed the same behavior for the magnitude of the frequency dependent fluxes as the nodal solution model. At very low frequencies where the delayed neutrons are the information carriers, the magnitude of the flux was very high. As the frequency increases the magnitude of the flux decreases until it reachs a plateau region, then at very high frequencies the prompt neutrons become dominant in the solution and the magnitude becomes very small.

The convergence of the analytical solution depends on the frequency as well as on the distance between the source and the observed point. At points far from the source, both the real and the imaginary parts of the flux converge

rapidly, for example, at the point (35, 35, 35) the solution converges when the summation limit equals 15, which is equivalent to 3375 terms. As the observed point gets closer to the source, the number of terms needed for convergence increases. At the source location, the solution never converges and continues to increase as the summation limit increases.

The frequency has different effects on the convergence of the real and the imaginary parts. At all frequencies, the imaginary part converges faster than the real part. Considering the imaginary part alone, it shows faster convergence at low frequencies. On the other hand, the real component converges faster at high frequencies.

C. Comparison of the Results

The ratio of analytical to nodal results was used to compare the two solutions. The flux values at points along a line inside the cube were investigated. To consider the whole cube, several lines, as shown in Figure 7.6 were chosen and the values of the fluxes at different points on these lines were calculated using both methods. Finally, the ratio between the solutions were calculated and plotted. Figure 7.7 through 7.10 shows the ratio between fluxes for ω = 10.0 rad/s while Figures 7.11 through 7.18 shows the ratio for ω = .05 and 1000 rad/s. The small circles on the graphs

indicates the points along the x-axis at which the ratio is calculated.

The ratio between the analytical solution and the nodal solution is found to be approximately unity. At points that are away from the source where the analytical solution had converged and the nodal solution is not affected by the source shape and size, the ratio is about 1.1. Far from the source both solutions will converge but the leakage from the nodal model is greater due to the finite source shape. Therefore, the analytical solution will give a higher flux and the ratio will be above one. At points closer to the source, the analytical solution has not converged and the nodal solution has the finite source effect. In this case, the ratio will include both effects and shows a greater divergence from unity.

The discontinuity of the plots at x = 32 cm, 50 cm and 68 cm as shown in Figure 7.7 indicates the effect of the node boundaries. Also at the node boundaries and for the line y = z = 32 cm, the effect of the node corners is clear. The line y = z = 32 cm is along the edge of several nodes and passes through node corners where the continuity of the flux and the current is not guaranteed.

Decreasing the size of the source in the nodal model resulted in an increase in the flux values at the source location. The size of the source was decreased using two

methods. First, by defining smaller nodes at the source location and second, by increasing the number of nodes that represent the reactor model. Although decreasing the node sizes around the source resulted in sharper peaks in the flux at the source location, it reduced the convergence speed of the solution and a larger number of iterations was required to get to an answer. Decreasing the source size by increasing the number of nodes also resulted in sharper peaks at the source location but the program execution time became a major concern. Table 7.1 shows the effect of the number of nodes and the number of iterations on the execution times on the National Advanced System/9160 computer (NAS), an IBM 370 compatible computer running under MVS/SP.

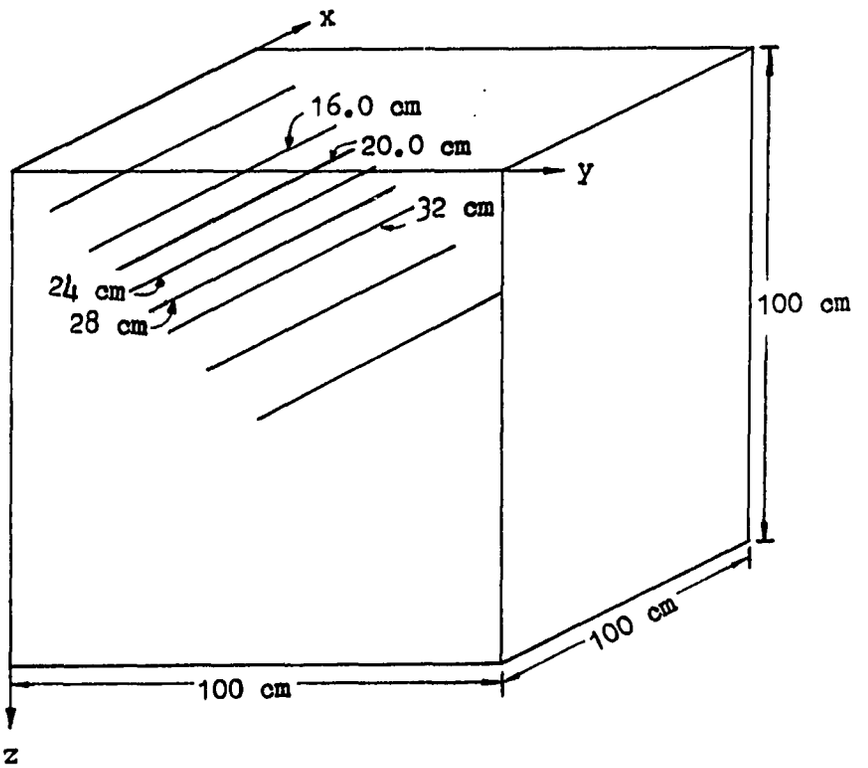

Figure 7.6. Locations inside the cube used to compare the nodal results with the analytical solution of the frequency dependent neutron diffusion equations

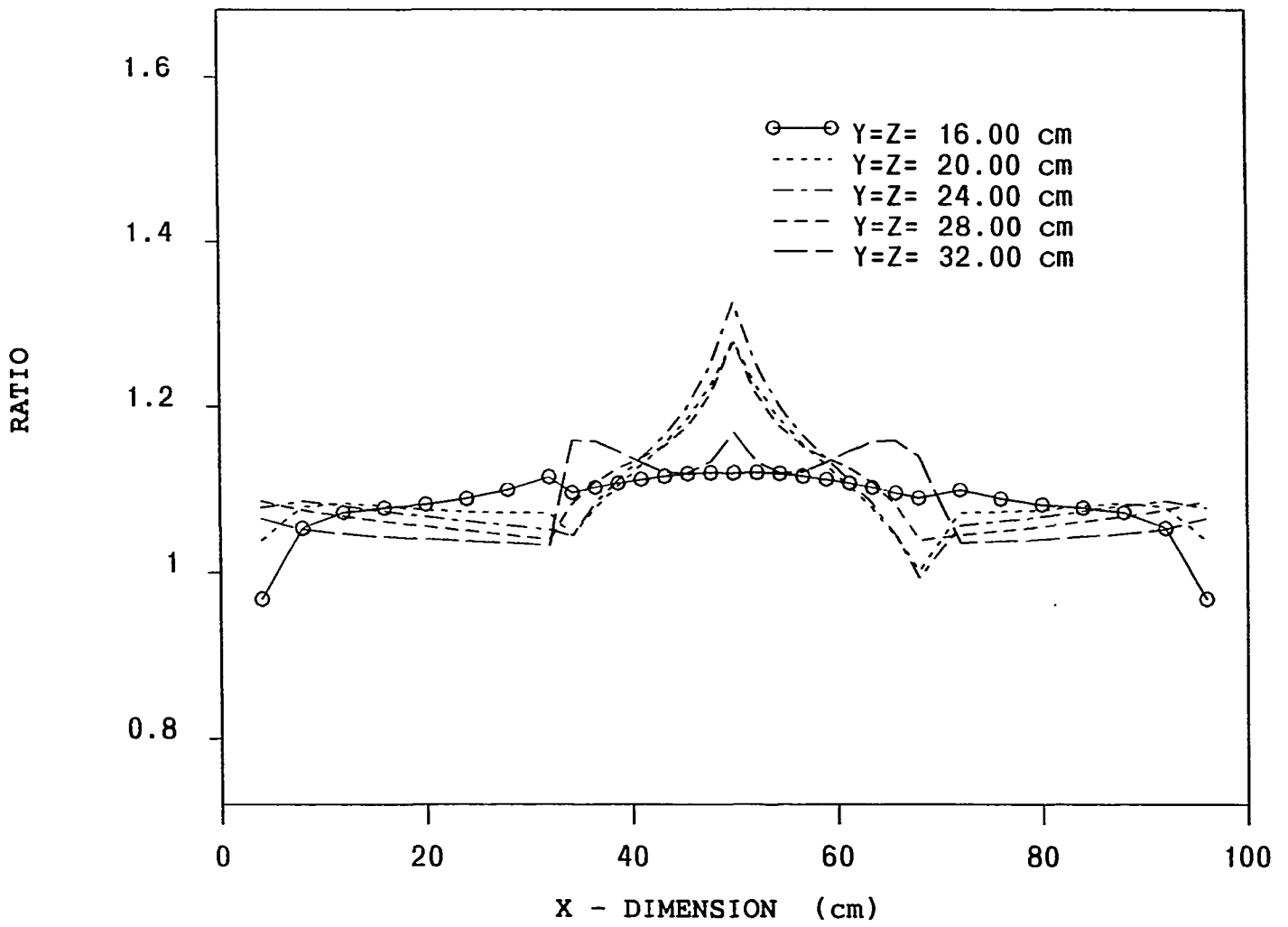

Figure 7.7. Ratio of analytical solution to nodal solution of the real fast flux at ω = 10 rad/s

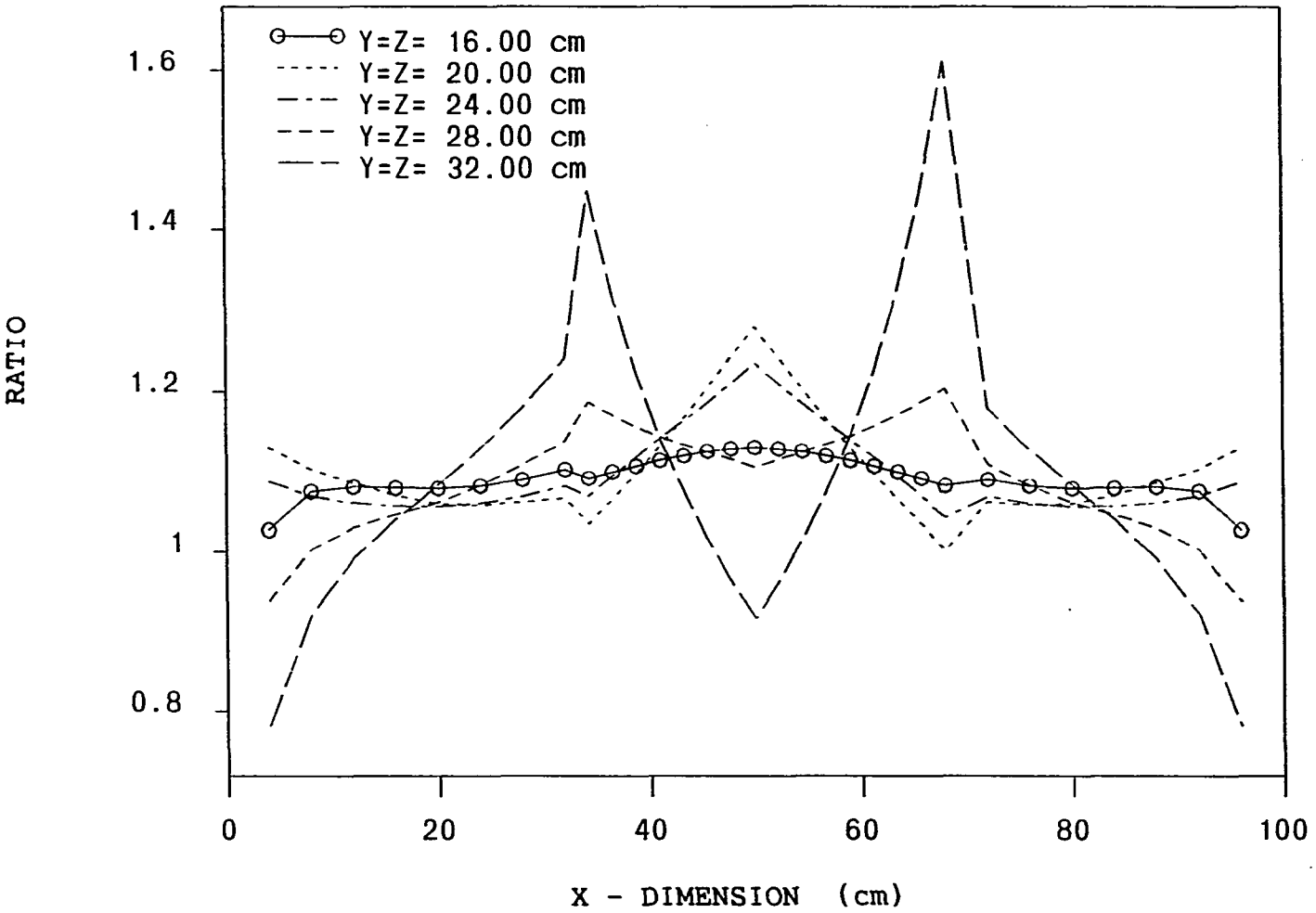

Figure 7.8. Ratio of analytical solution to nodal solution of the real thermal flux at ω = 10 rad/s

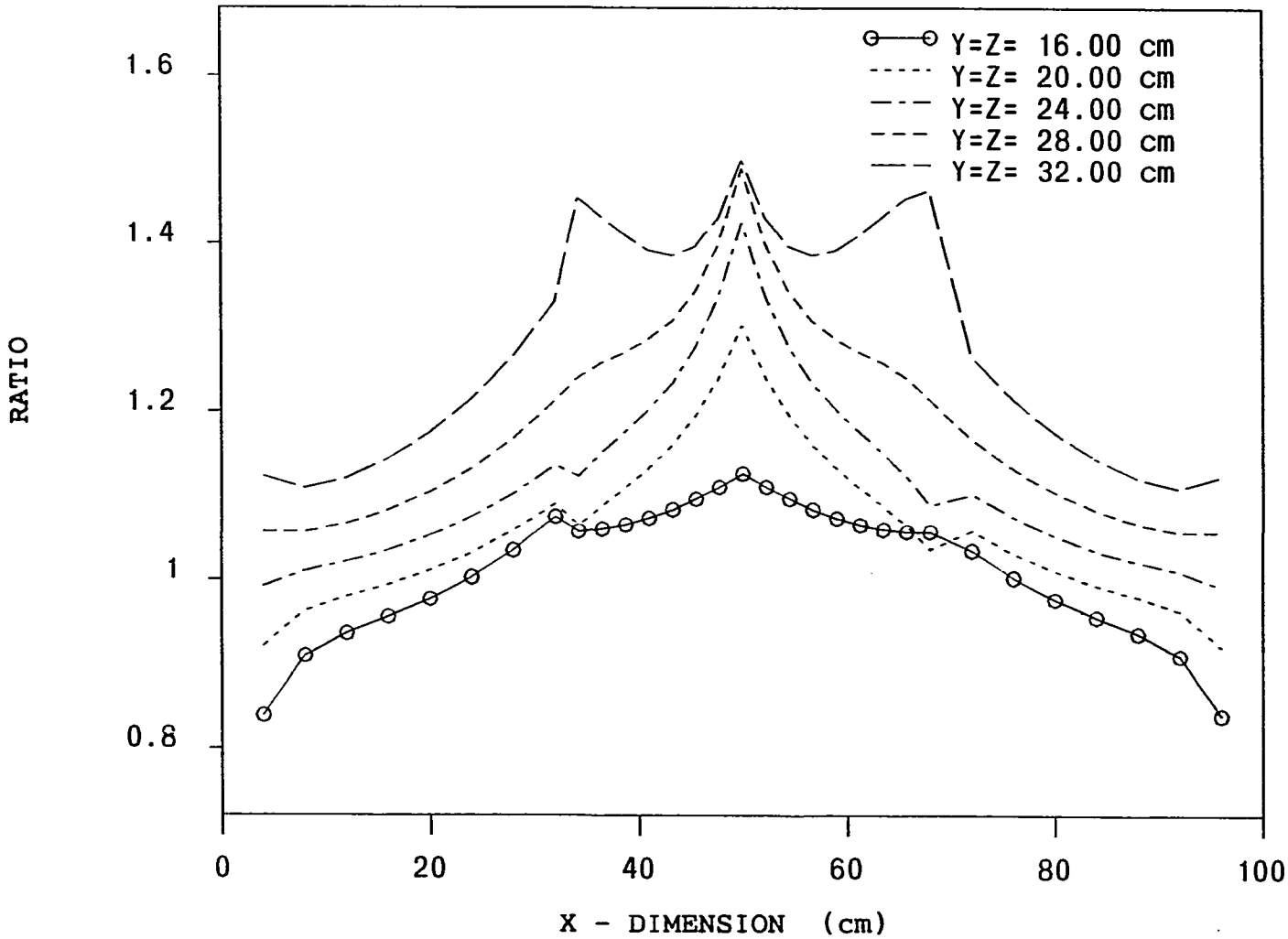

Figure 7.9. Ratio of analytical solution to nodal solution of the imaginary fast flux at ω = 10 rad/s

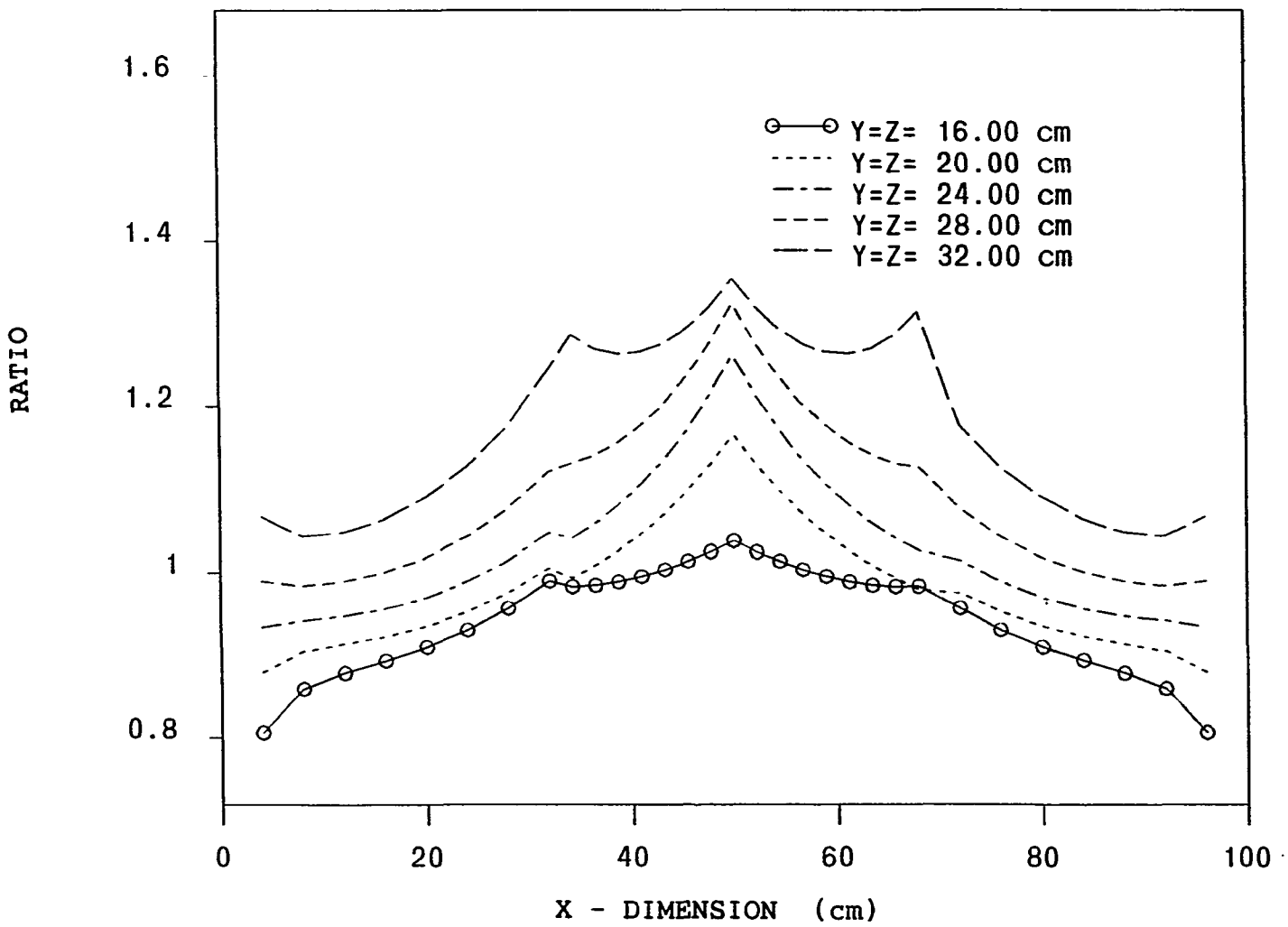

Figure 7.10. Ratio of analytical solution to nodal solution of the imaginary thermal flux at ω = 10 rad/s

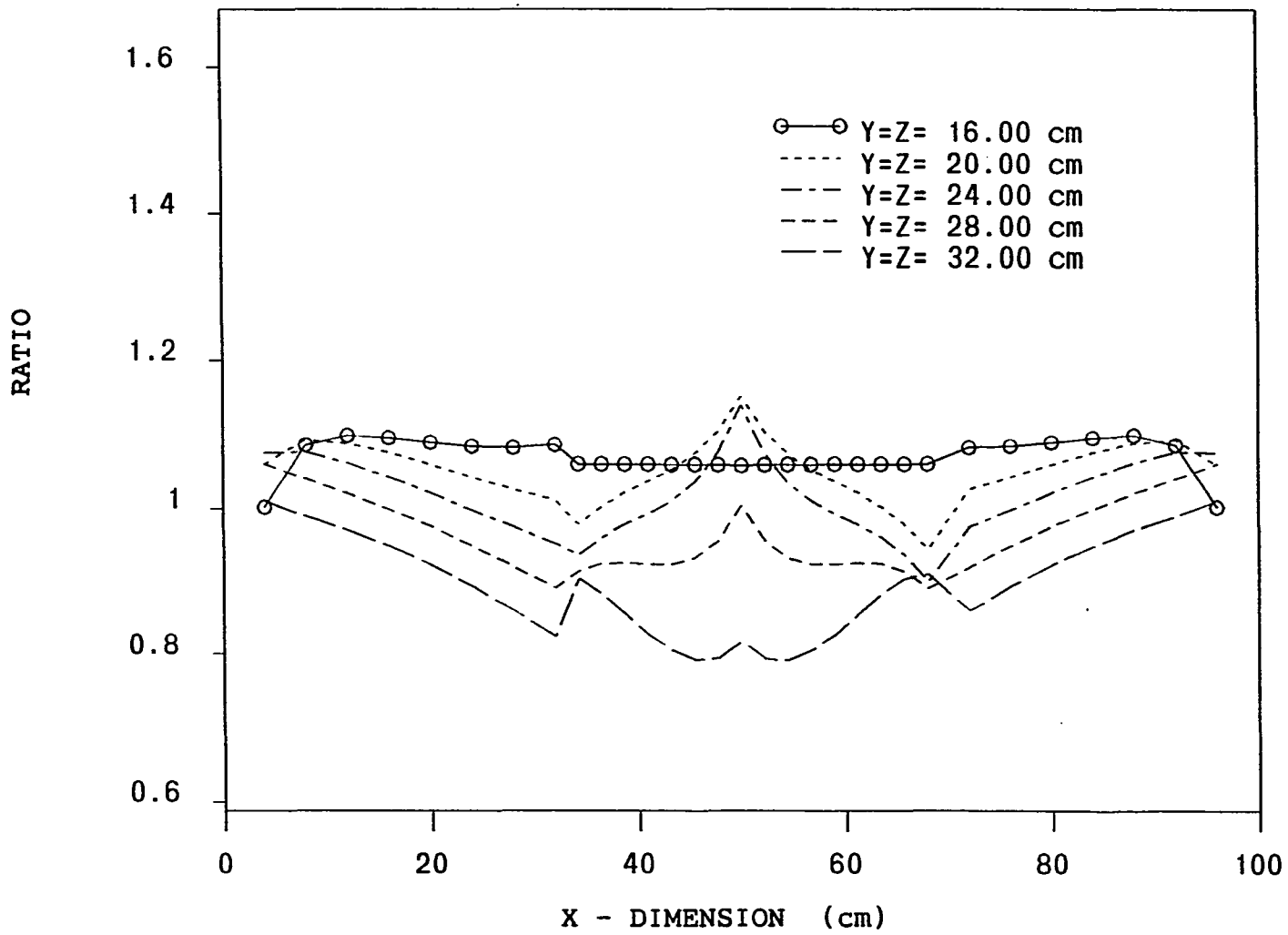

Figure 7.11. Ratio of analytical solution to nodal solution of the real fast flux at ω = .05 rad/s

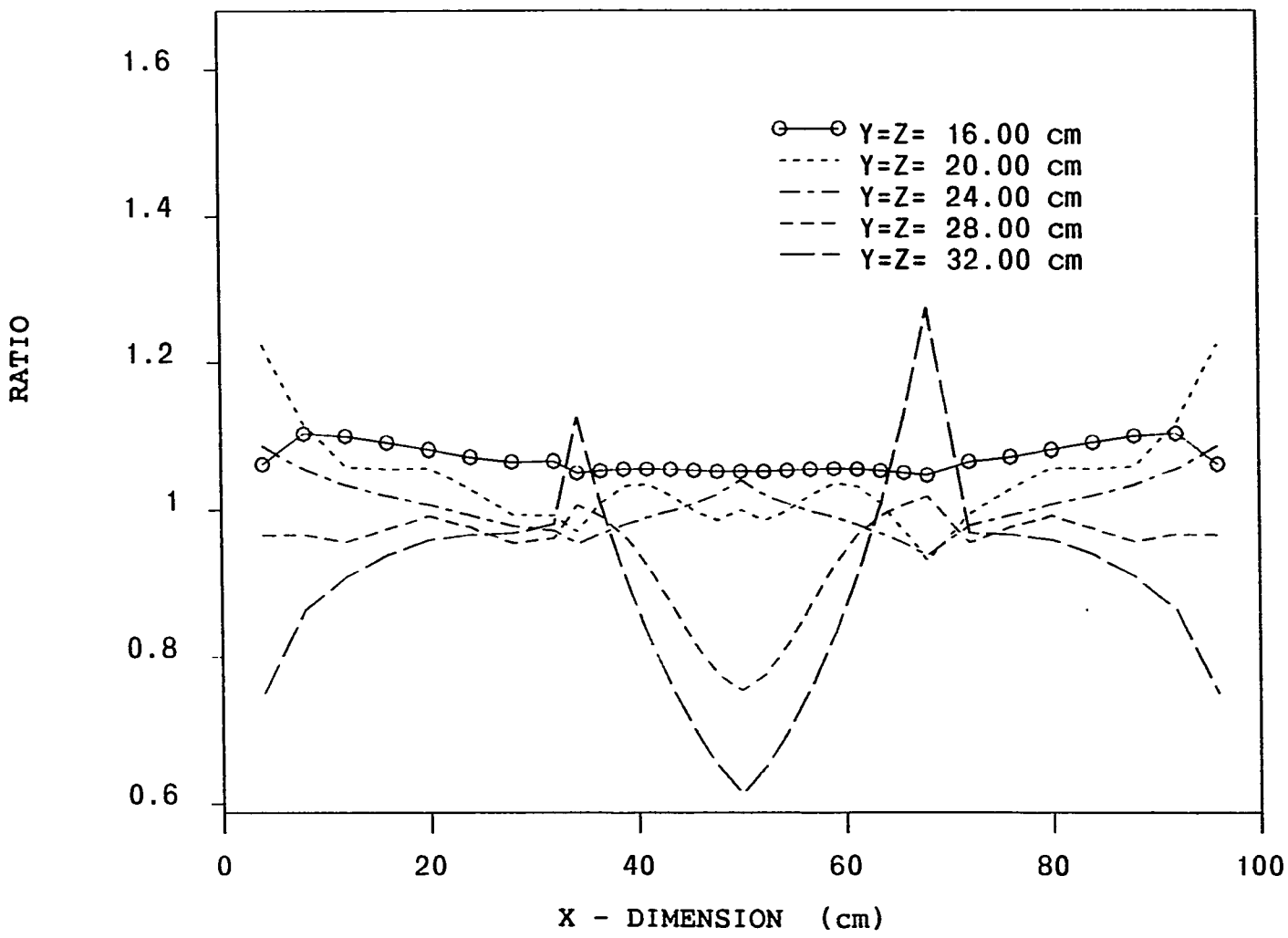

Figure 7.12. Ratio of analytical solution to nodal solution of the real thermal flux at ω = .05 rad/s

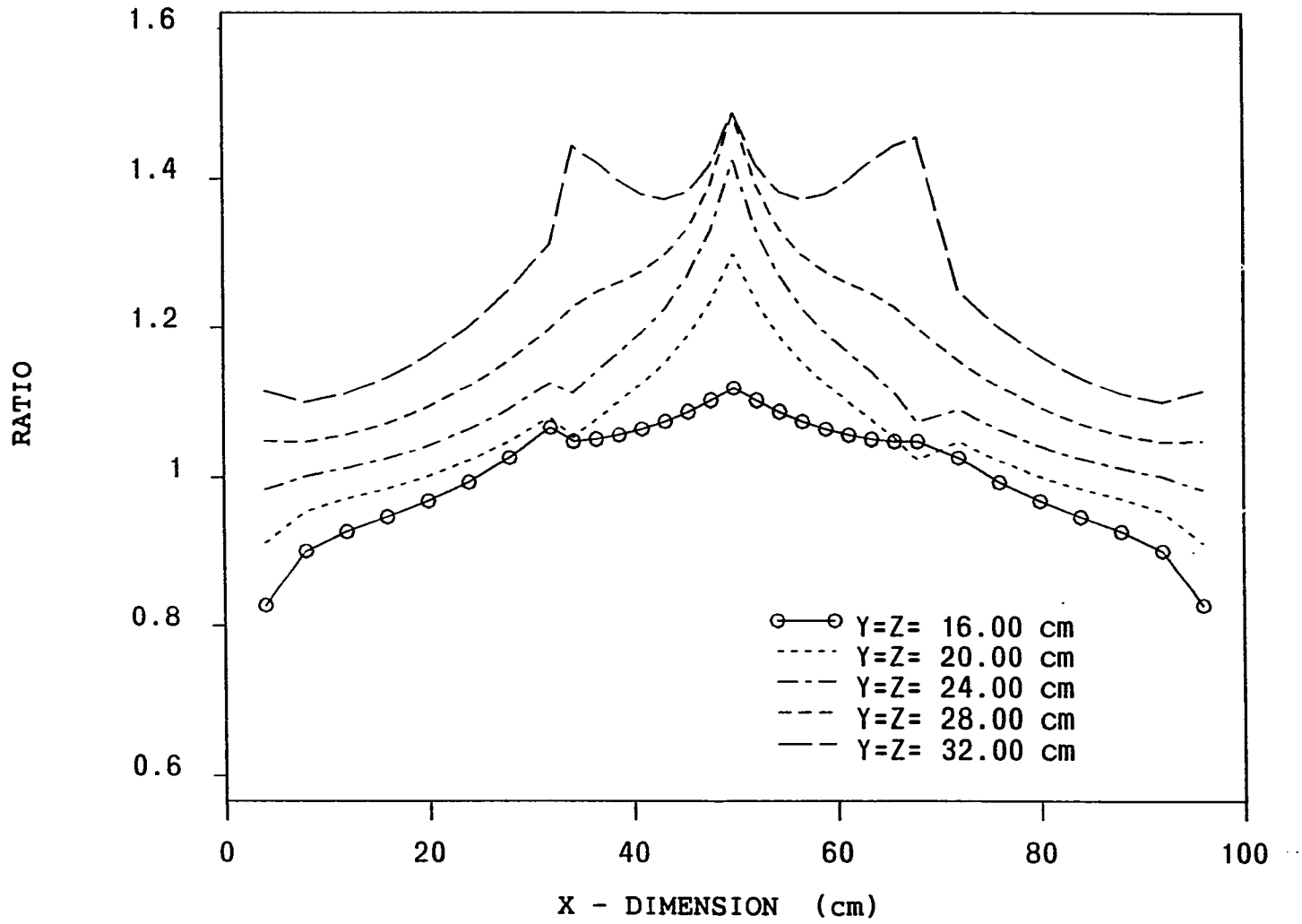

Figure 7.13. Ratio of analytical solution to nodal solution of the imaginary fast flux at ω = .05 rad/s

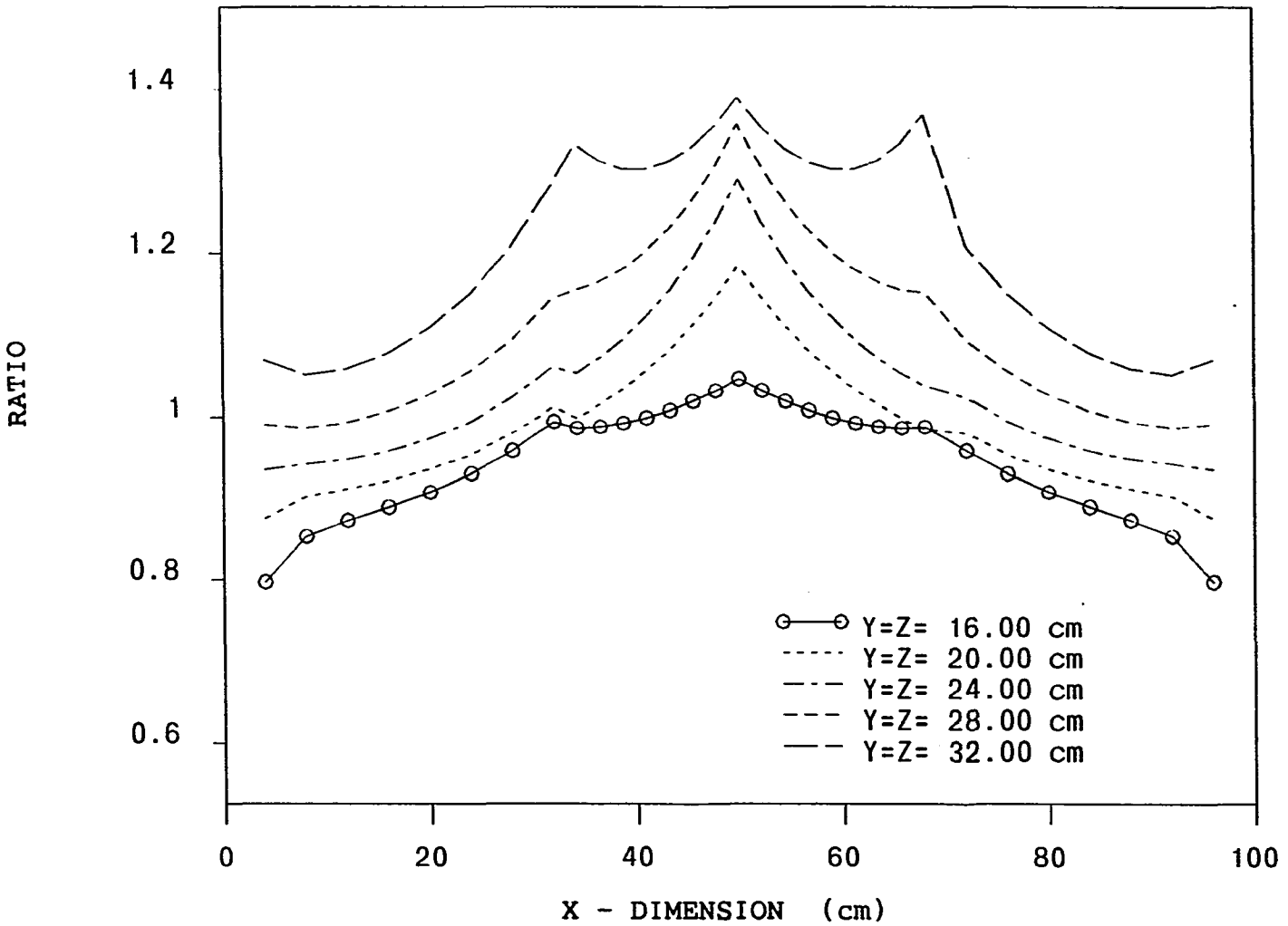

Figure 7.14. Ratio of analytical solution to nodal solution of the imaginary thermal flux at ω = .05 rad/s

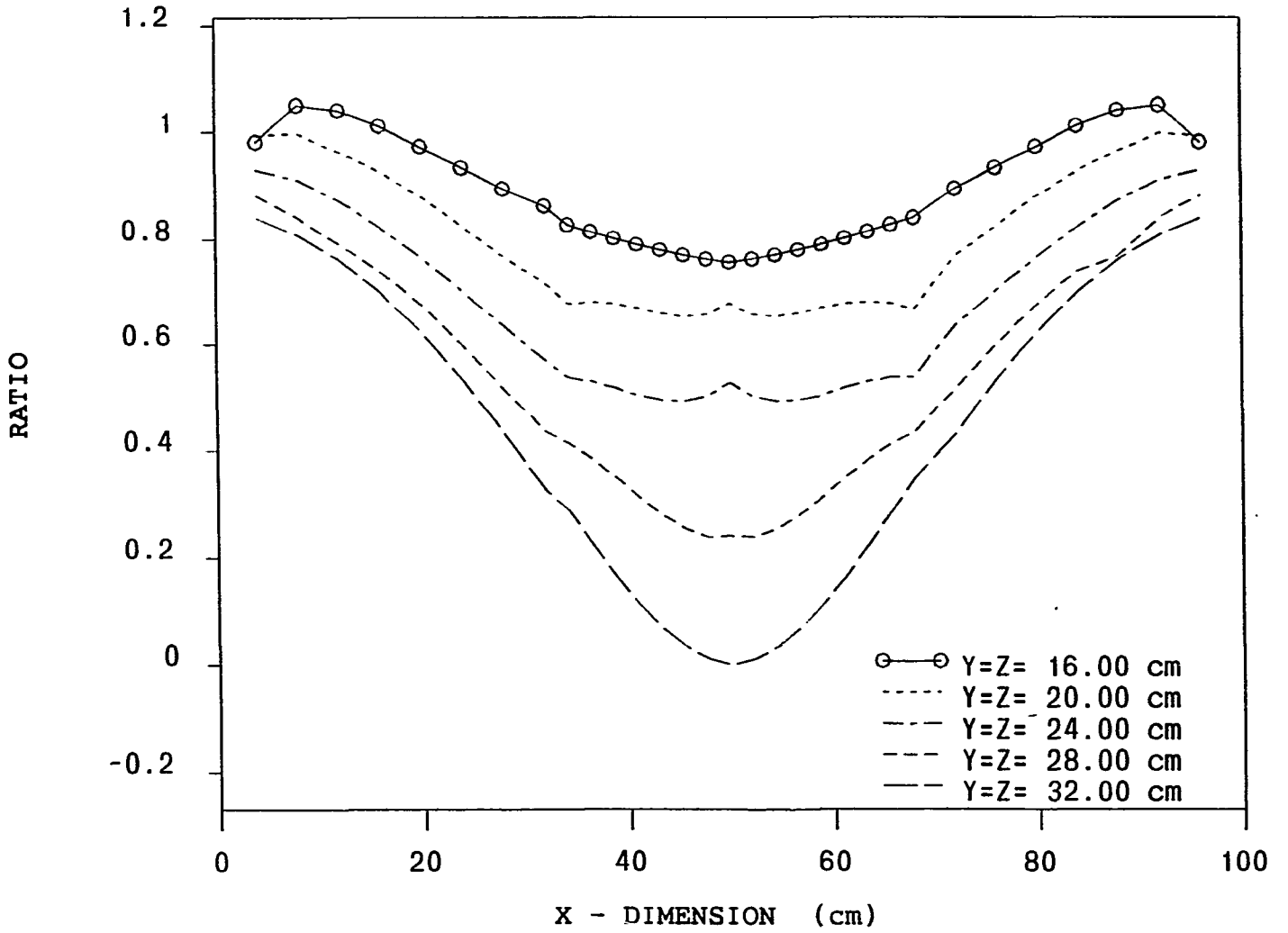

Figure 7.15. Ratio of analytical solution to nodal solution of the real fast flux at ω = 1000 rad/s

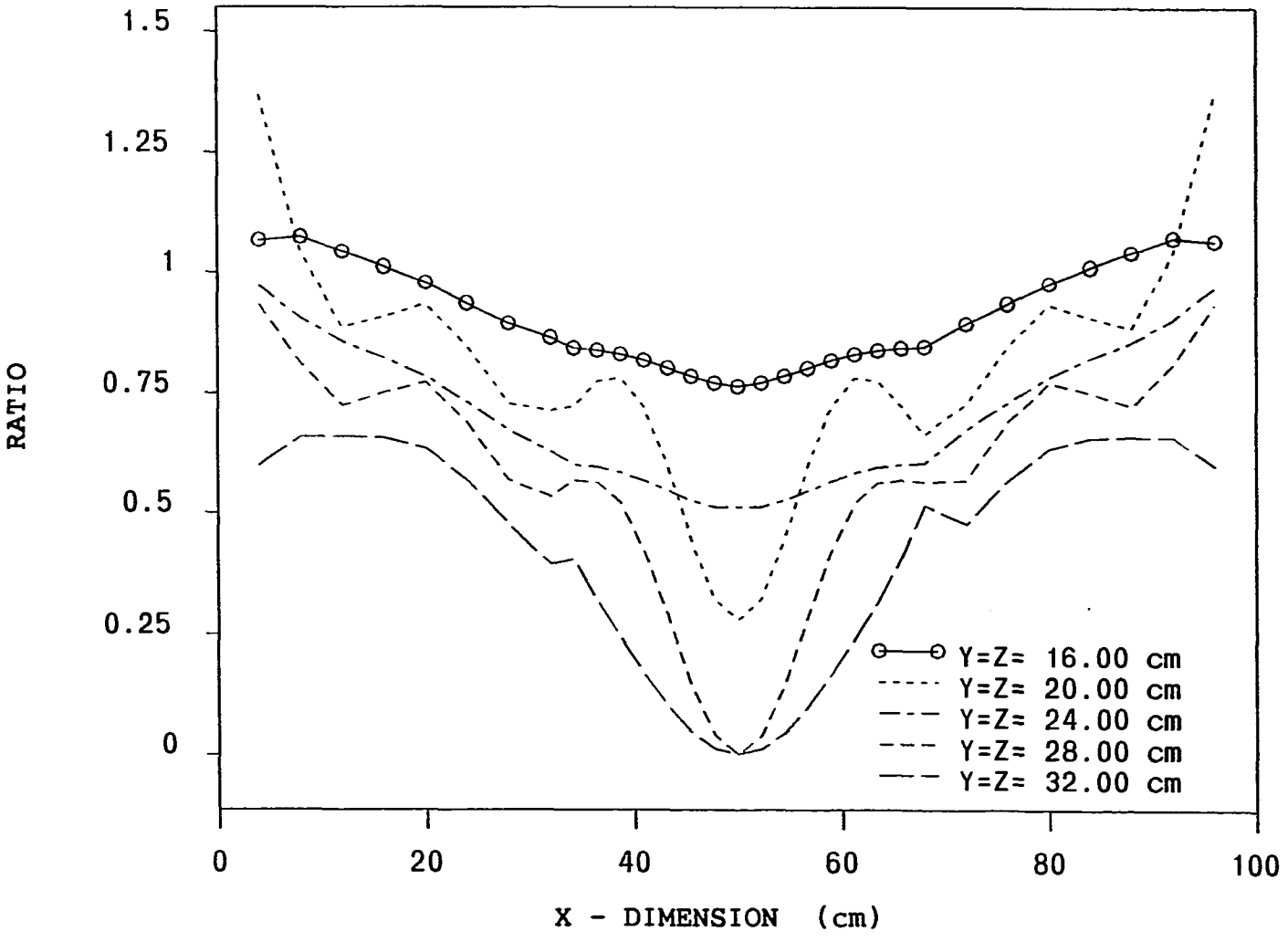

Figure 7.16. Ratio of analytical solution to nodal solution of the real thermal flux at ω = 1000 rad/s

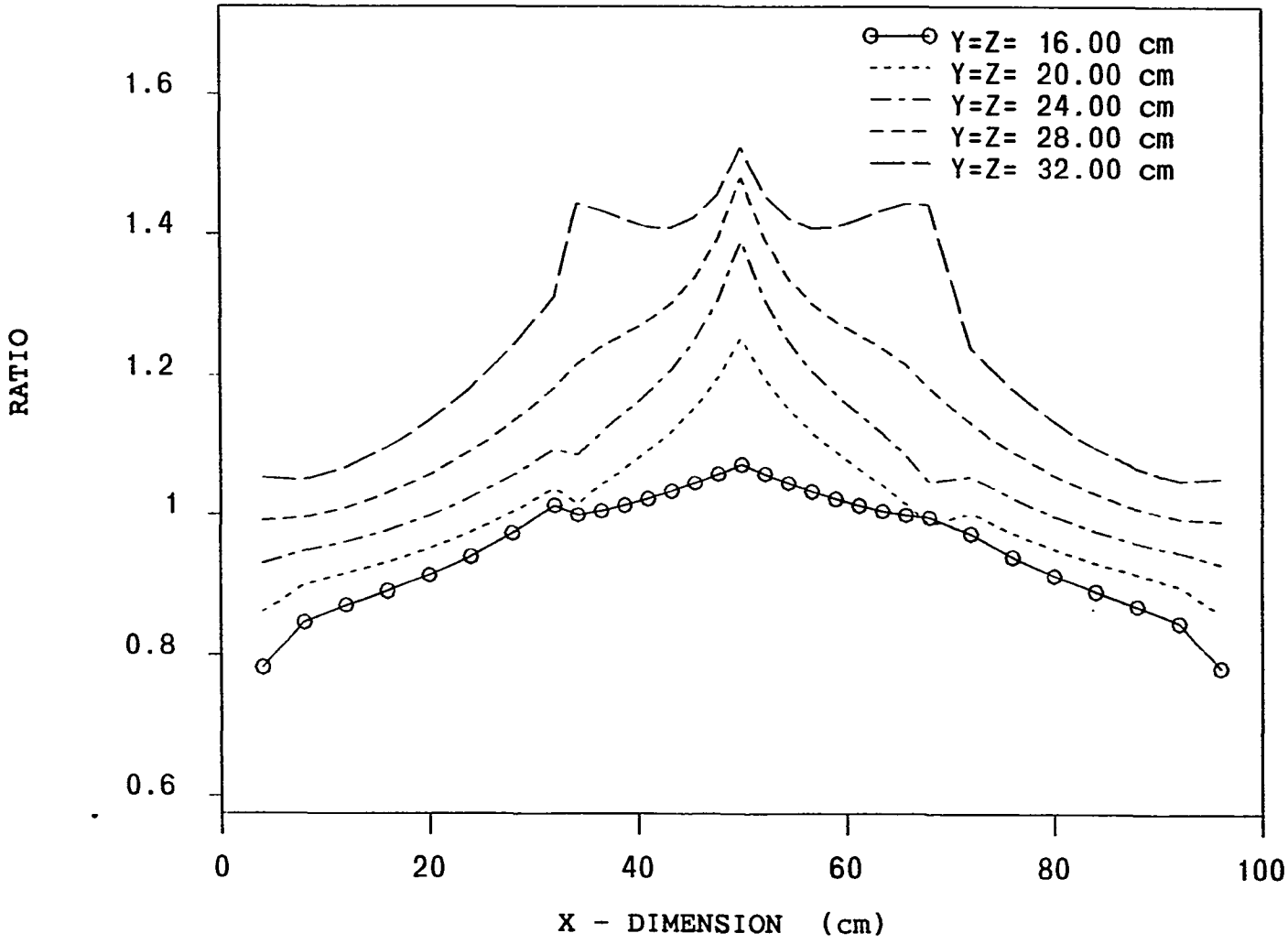

Figure 7.17. Ratio of analytical solution to nodal solution of the imaginary fast flux at ω = 1000 rad/s

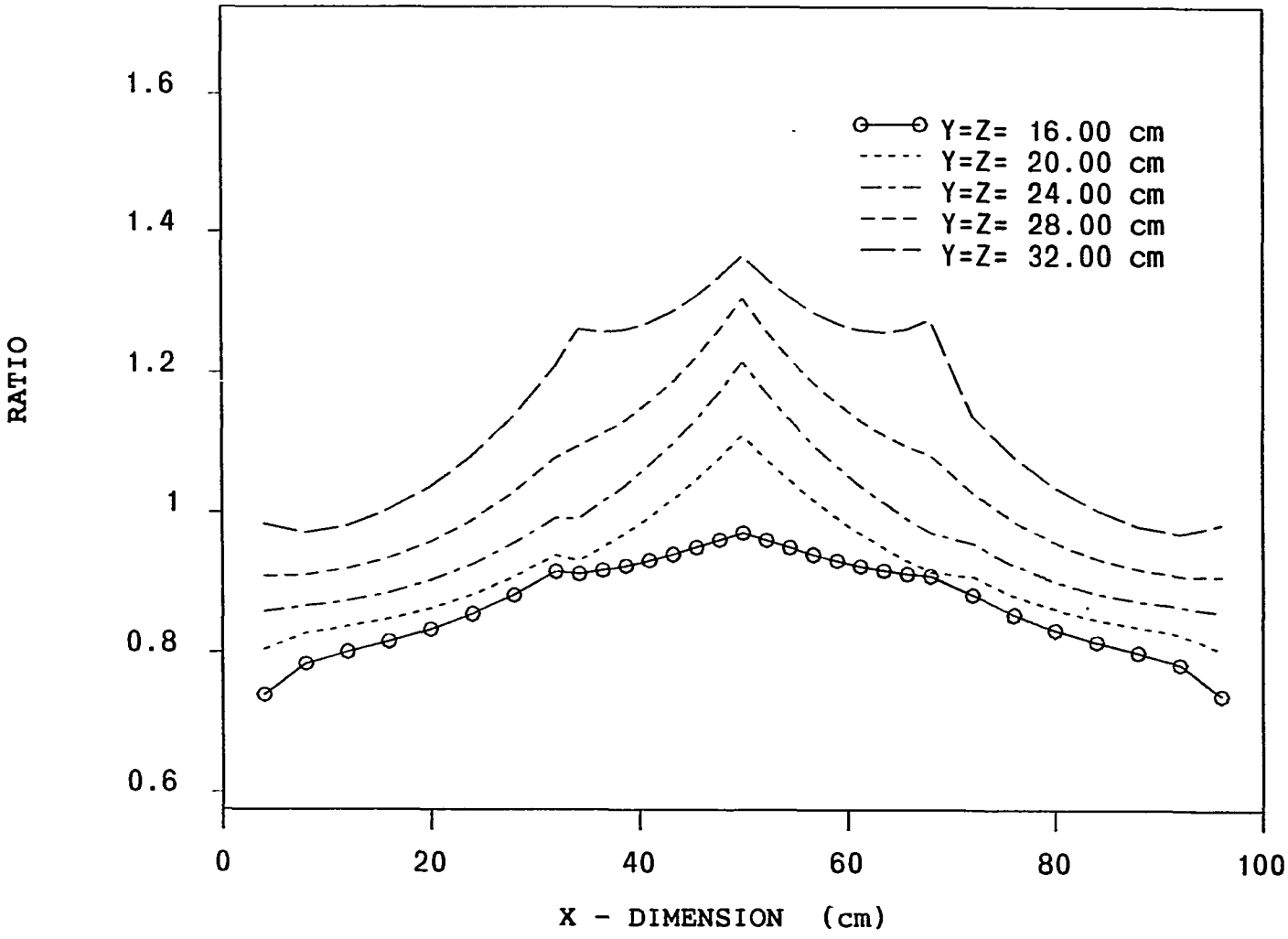

Figure 7.18. Ratio of analytical solution to nodal solution of the imaginary thermal flux at ω = 1000 rad/s

VIII. CONCLUSIONS

The objective of this research was to develop a three-dimensional nodal code that could be used to calculate the Fourier transformed regular or adjoint flux in a reactor.

A three-dimensional multigroup nodal code that requires very simple modifications to accept the frequency dependent equations was used for flux calculations. The major effort of this research was directed to the establishment of an analytical solution that can be used to verify the nodal code results. The results obtained from the nodal code and its comparison with the analytical solution support the following conclusions:

1. The nodal code is capable of predicting the general behavior of the Fourier transformed frequency dependent fluxes. In the plateau region of the zero power transfer function, the real part of the fluxes was very large in magnitude compared to the imaginary part and at very high and very low frequencies, the imaginary part was larger in magnitude than the real part. Moreover, the real and the imaginary parts have opposite signs and each sign depends upon the sign of the source.
2. The source representation as three intersecting

surfaces in the nodal model caused a divergence between the nodal and analytical results. The comparison was better when observed points were far from the source. Therefore the source size must be kept as small as possible for accurate results.

3. Increasing the number of nodes in the nodal model has two major effects. First, it reduces the size of the source, which is an advantage, on the other hand, it increases the computation time
4. Decreasing the size of the nodes adjacent to the source slows down convergence. Therefore, the problem requires a larger number of iterations to reach a converged solution.
5. The code was applicable for the frequency range of interest (0.1 Hz through few hundred Hz).

The nodal computer code can be used to solve the Fourier transformed adjoint equations for a localized source in a reactor, provided that the proper number of nodes and node sizes are used.

IX. SUGGESTIONS FOR FUTURE WORK

The presented work showed the validity of using the nodal numerical model for noise analysis over a simple geometry. The next step would be to apply the method to a realistic reactor model. Thus one could compare results obtained by the model with experimental data obtained from a reactor with small sources or vibrating elements.

Several simplifications and approximations were employed in applying this model. Therefore, examining other models with fewer approximations would be an interesting task.

The following points are suggestions for extending this investigation:

1. Use three or more neutron energy groups, several delayed neutron groups, and other Legendre expansion orders to more accurately model current reactor systems.
2. Perturb all material properties rather than just the absorption cross section.
3. Increase the number of nodes in order to decrease node sizes around the source location and to get a better approximation for the point source.
4. Test different material compositions and heterogeneous reactors.

5. Improve the convergence by using accelerated convergence algorithms and possible variation of the interface parameter θ.

X. LITERATURE CITED

1. M. Al-Ammar, use of local-global ratio in detecting component vibration in reactors, Ph.D. dissertation, Iowa State University, 1981 (unpublished).

2. G. Th. Analytis, Three-group three-dimensional analysis of the random neutron field in bare homogeneous reactors and the concepts of local and global neutron noise, Annals of Nucl. Energy 9, 53 (1982).

3. M. Antonopoulos-Domis, On the space dependence of neutron density noise and the problem of malfunction localization, Annals of Nucl. Energy 8, 91 (1981).

4. R. M. Ball and J. M. Huzdovich, Light water reactor diagnostic experience using noise analysis, Nuclear safety 22, 43 (1981).

5. K. Behringer, G. Kosály and Lj. Kostić, Theoretical investigation of the local and global components of the neutron-noise field in boiling water reactor, Nucl. Sci. Engr. 63, 306 (1977).

6. K. Behringer and R. Crowe, Practical application of neutron noise analysis at boiling water reactors, Atomkernenergie 38, 47 (1981).

7. C. E. Cohn, R. J. Johnson and R. N. Macdonald, Calculating space-dependent reactor transfer functions using static techniques, Nucl. Sci. Engr. 26, 198 (1966).

8. R. Courant and D. Hilbert, Methods of Mathematical Physics (Interscience Publishers, New York, 1965).

9. H. Dam, Neutron noise in boiling water reactors, Atomkernenergie 27, 8, (1976).

10. H. Dam, On the adjoint space in reactor noise theory, Annals of Nucl. Energy 4, 185 (1977).

11. M. Edelmann, Some considerations on neutron instrumentation requirements for malfunction diagnosis in power reactors using noise analysis techniques, Annals of Nucl. Energy 2, 261 (1975).

12. Y. Gotoh and H. Yasuda, Investigation of space-dependent neutron flux fluctuation excited by a strong absorber, Annals of Nucl. Energy 10, 589 (1983).

13. E. Greenspan, On the adjoint space in reactor theory, Annals of Nucl. Energy 3, 323 (1976).

14. W. J. Hennessy, An investigation of the two-dimensional neutron noise field generated by a moving neutron absorber using UTR-10 reactor. M.S. thesis, Iowa State University, 1983 (unpublished).

15. W. J. Hennessy, R. A. Danofsky and R. A. Hendrickson, some observations of the two-dimensional neutron noise field generated by a moving neutron absorber located in the reflector region of a low power reactor, Nucl. Sci. Engr. 88, 513 (1984).

16. A. F. Henry, Nuclear Reactor Analysis (The MIT Press, Cambridge, 1982).

17. D. L. Hetrick, Dynamics of Nuclear Reactors (The University of Chicago Press, Chicago, 1971).

18. L. R. Huang, Use of adjoint space model for predicting the response of a neutron detector to core parametric fluctuations, Ph.D. thesis, Iowa State University, 1979 (unpublished).

19. D. E. Jeffers, Spatial transfer function of a two core reactor, Atomkernenergie 16, 129 (1970).

20. G. Kosály and M. M. Williams, Point theory of the neutron noise induced by inlet temperature fluctuations and random mechanical vibrations, Atomkernenergie 18, 203 (1971).

21. G. Kosály and L. Meskó, Remarks on the transfer function relating inlet temperature fluctuations to neutron noise, Atomkernenergie 20, 33 (1972).

22. G. Kosály, L. Meskó and I. Pázsit, Investigation of the possibility of using static calculations (adiabatic-approximation) in the theory of reactor noise, Annals of Nucl. Energy 4, 79 (1977).

23. G. Kosály, Noise investigations in boiling water and pressurized water reactors, Prog. Nucl. Energy 5, 145 (1980).

24. S. J. Lee and R. W. Albrecht, The use of neutronic fluctuations to locate a vibrating control rod in a pressurized water reactor model, Nucl. Sci. Engr. 83, 427 (1983).

25. S. J. Lee, Multi-group diffusion modeling of at-power neutron noise, Atomkernenergie 43, 37 (1983).

26. J. Lewins, Importance - The Adjoint Function (Pergamon Press, New York, 1965).

27. I. Pázsit, Investigation of space-dependent noise induced by a vibrating absorber, Atomkernenergie 30, 29 (1977).

28. I. Pázsit, Two-group theory of noise in reflected reactors with application to vibrating absorbers, Annals of Nucl. Energy 5, 185 (1978).

29. I. Pázsit and G. Th. Analytis, Theoretical investigation of neutron noise diagnostics of Two-dimensional control rod in a PWR, Annals of Nucl. Energy 7, 171 (1980).

30. I. Pázsit and O. Glöckler, On the neutron noise diagnostics of pressurized water reactor control rod vibrations. I. Periodic vibrations, Nucl. Sci. and Engr. 85, 167 (1983).

31. I. Pázsit and O. Glöckler, On the neutron noise diagnostics of pressurized water reactor control rod vibrations. II. Stochastic vibrations, Nucl. Sci. and Engr. 88, 77 (1984).

32. A. F. Rohach, A polynomial nodal model using Legendre expansions, Annals of Nucl. Energy 13, 57 (1986).

33. A. F. Rohach, A Legendre polynomial nodal model for two dimensional diffusion problem, Annals of Nucl. Energy 13, 549 (1986).

34. A. F. Rohach, Department of Nuclear Engineering, Iowa State University, Private Communications, 1987.

35. K. Saito and M. Otsuka, Transfer function and power spectral density in a zero power reactor, Journal of Nucl. Sci. and Tech. 3, 45 (1966).

36. K. Saito, On the theory of power reactor noise-I, Annals of Nucl. Energy 1, 31 (1974).

37. K. Saito, On the theory of power reactor noise-II, Annals of Nucl. Energy 1, 107 (1974).

38. K. Saito, On the theory of power reactor noise-III, Annals of Nucl. Energy 1, 209 (1974).

39. V. D. Schwalm, Some remarks on failure detection in nuclear power reactors by noise measurements, Atomkernenergy 19, 263 (1972).

40. F. J. Sweeney, J. P. A. Renier, Sensitivity of detecting in-core vibration and boiling in pressurized water reactors using ex-core neutron detectors, NUREG/CR-2996 (ORNL/TM-8549) (1984).

41. J. A. Thie, core motion monitoring, Nucl. Technol. 45, 5 (1979).

42. M. R. Wagner, Current trends in multi-dimensional static calculations, CONF 750413 Vol. I, 1 (1975).

43. D. Wach and G. Kosály, Investigation of the joint effect of local and global driving sources in incore neutron noise measurements, Atomkernenergie 23, 244 (1974).

44. A. M. Weinberg and H. C. Schweinler, Theory of oscillating absorber in a chain reactor, Phys. Rev. 74, 851 (1948).

45. M. M. R. Williams, Reactivity changes due to the random vibration of control rods and fuel elements, Nucl. Sci. Engr. 40, 144 (1970).

46. M. M. R. Williams, Random Process in Nuclear Reactors (Pergamon Press, Oxford, England, 1974).

XI. ACKNOWLEDGMENTS

The author wishes to express his special appreciation to Dr. R. A. Danofsky and Dr. A. F. Rohach for many helpful discussions, suggestions, and encouragement throughout the course of this research. In addition, the author would like to thank King Abdulaziz University in Jeddah, as well as the Saudi Arabian Educational Mission in Washington, D.C. for their financial support. Finally, the author is deeply grateful to his parents, wife, and children for their understanding through the years of study.

XII. APPENDIX A: THE NODAL CODE

The nodal code, which is a multigroup, multiregion, three-dimensional neutron diffusion code, has these modifications as applied to this research :

1. The external source strength which appears as (S) neutrons/second is considered as (48 * S) neutrons/second inside the program.
2. The code accepts negative fluxes and upscattering cross sections.
3. Flux groups 1,2,3 and 4 represent the fast real, thermal real, fast imaginary and thermal imaginary equations respectively.
4. Neutron production by fission is only allowed in the real groups and all other coupling between groups are considered as scattering.
5. All scattering cross sections that did not appear in the original two-group frequency dependent neutron diffusion equations are accounted for in the absorption cross section.
6. The coupling between real and imaginary parts include both up and down-scattering.

The input data generating program is written for two neutron energy groups and can be modified easily for more neutron groups.

A. Input Data Description

BETA	Delayed neutron fraction, β
LAMBDA	Decay constant for delayed neutron precursors, λ
V	neutron speed, v
W	Frequency, ω
NRMIN	Minimum number of regions
NRMAX	Maximum number of regions
NMAT	Number of microscopic cross sections
NOG	Number of neutron groups
CHI	Fission neutron fraction for each group, χ
D	Diffusion coefficient, D
SIG	Absorption cross section, Σ_a
NSIGF	Fission cross section, $\nu\Sigma_f$
SIGS	Scattering cross section, Σ_s

B. Input Data Generating Program

```
      REAL CHI(4),D(4),NSIGF(4),SIG(4),KSIG(4)
      REAL SIGS(4,4),V(4),LAMBDA,NSIG1,NSIG2

      OPEN(UNIT=7,TYPE='NEW',NAME='NXSCTN.DAT')
      OPEN(UNIT=8,TYPE='OLD',NAME='AR.DAT')

      READ(8,*)BETA,LAMBDA,V(1),V(2),W
      DUM=BETA*LAMBDA/(LAMBDA*LAMBDA+W*W)
      HR=1.0-BETA+LAMBDA*DUM
      HI=-W*DUM
      HC=(HR*HR+HI*HI)/HR
      WV1=W/V(1)
      WV2=W/V(2)

      READ(8,*)NRMIN,NRMAX,NMAT,NOG
      NOGG=NOG*2
      WRITE(7,*)NRMIN,NRMAX,NMAT,NOGG

      READ(8,*)(CHI(G),G=1,NOG)
      WRITE(7,*)(CHI(G),G=1,NOGG)

      DO 150 NR=1,NRMAX

        READ(8,160)DUMMY
160     FORMAT(A4)
        WRITE(7,160)

          DO 170 G=1,NOG
          READ(8,*)D(G),NSIGF(G),SIG(G),KSIG(G)
170       CONTINUE

          DO 180 L=1,NOG
          READ(8,*)(SIGS(H,G),G=1,NOG)
180       CONTINUE

        D(3)=D(1)
        D(4)=D(2)
        KSIG(3)=KSIG(1)
        KSIG(4)=KSIG(2)
        NSIG1=NSIGF(1)
        NSIG2=NSIGF(2)
        NSIGF(1)=NSIGF(1)*HR
        NSIGF(2)=NSIGF(2)*HR
        NSIGF(3)=0.0
        NSIGF(4)=0.0
        SIGS(1,3)=WV1-NSIG1*CHI(1)*HI
        SIGS(1,4)=-NSIG2*CHI(1)*HI
        SIGS(2,3)=-NSIG1*CHI(2)*HI
        SIGS(2,4)=WV2-NSIG2*CHI(2)*HI
        SIGS(3,1)=-WV1+NSIG1*CHI(1)*HI
```

```
      SIGS(3,2)=NSIG2*CHI(1)*HI
      SIGS(3,3)=0.0
      SIGS(3,4)=NSIG2*CHI(1)*HR
      SIGS(4,1)=NSIG1*CHI(2)*HI
      SIGS(4,2)=-WV2+NSIG2*CHI(2)*HI
      SIGS(4,3)=SIGS(2,1)+NSIG1*CHI(2)*HR
      SIGS(4,4)=0.0
      SIG(4)=SIG(2)-SIGS(1,4)-SIGS(2,4)-SIGS(3,4)-NSIG(2)
     &*CHI(2)*HR+SIGS(1,2)
      SIG(3)=SIG(1)-SIGS(1,3)-SIGS(2,3)-SIGS(4,3)-NSIG(1)
     &*CHI(1)*HR+SIGS(2,1)
      SIG(2)=SIG(2)-SIGS(3,2)-SIGS(4,2)
      SIG(1)=SIG(1)-SIGS(3,1)-SIGS(4,1)

      WRITE(7,*)D(1),NSIGF(1),SIG(1),KSIG(1)
      WRITE(7,*)D(2),NSIGF(2),SIG(2),KSIG(2)
      WRITE(7,*)D(3),NSIG(3),SIG(3),KSIG(3)
      WRITE(7,*)D(4),NSIG(4),SIG(4),KSIG(4)
      WRITE(7,9)((SIGS(I,J),J=1,4),I=1,4)
9     FORMAT(4E18.10)
150   CONTINUE

      STOP
      END
```

C. Sample Input File

```
0.0065   0.1   3.6E6   2.2E5   10.0
1   1   0   2
1.0   0.0
1.5   0.00   0.01   0.00
0.4   0.14   0.08   0.00
0.00   0.00
0.02   0.00
```

D. Sample Output File

```
1   1   0   4
1.0   0.0   0.0   0.0
1.5   0.00   1.00E-2   0.00
0.4   0.139   8.01E-2   0.00
1.5   0.00   1.00E-2   0.00
0.4   0.00   -5.92E-2   0.00
 0.00        0.00        0.33E-5    0.91E-5
 0.20E-1     0.00        0.00       0.46E-4
-0.33E-5    -0.91E-5     0.00       0.139
 0.00       -0.46E-4     0.20E-1    0.00
```

XIII. APPENDIX B: THE COMPUTER PROGRAM FOR THE ANALYTICAL SOLUTION

The following is a description of the input data required for the three-dimensional analytical solution program which solves the Fourier transformed neutron diffusion equations. A listing of the program and a sample input data file are also provided. Special features of the program are listed below:

1. The analytical solution is for a cubic reactor model with one point source located anywhere inside the reactor.
2. The solution can be calculated either for the x-y plane at a specific z level or along the x-direction for certain values of y and z.
3. The analytical solution can be calculated using three methods. These methods are the sine summation formula, the two exponential terms solution and the eight exponential terms solution.
4. In order to use the residue theorem, the appropriate poles must be selected. For this research the selection is made with the help of Figure B.1. It shows the phase of each of the four denominator roots at different frequencies.

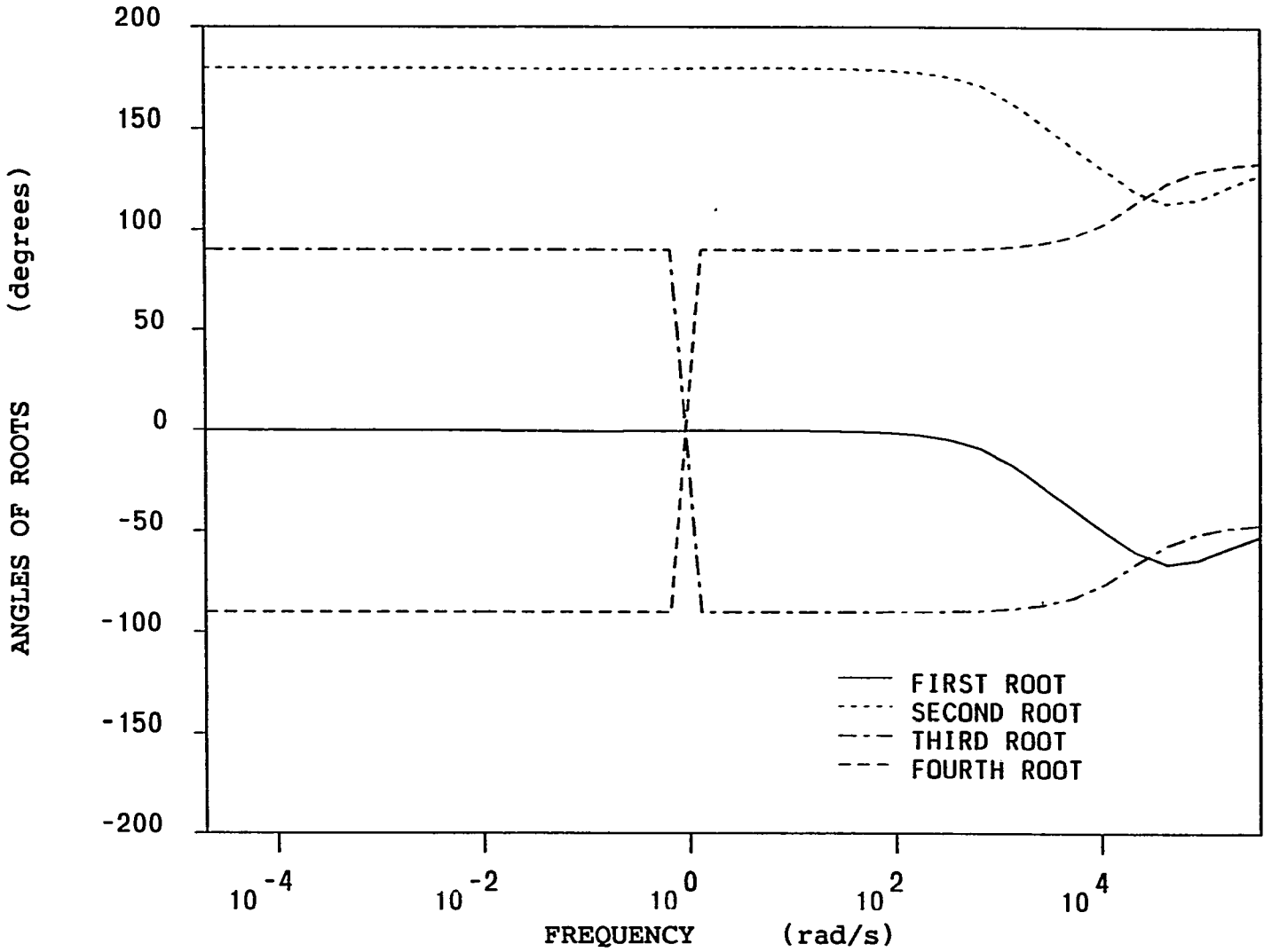

Figure B.1. Location of B_s, the roots of equation 5.21, at different frequencies

A. Input Data Description

NOG	Number of neutron energy groups
IOPT1	Solution options
	= 1 To calculate the solution for the x-y plane
	= 2 To calculate the solution along x direction
IOPT2	Solution options
	= 0 For the triple sine summation solution
	= 2 For the two exponential terms solution
	= 8 For the eight exponential terms solution
D	Diffusion coefficient, D
SIG	Absorption cross section, Σ_a
SIGF	Fission cross section, $\nu\Sigma_f$
V	Neutron speed, v
SIGS	Scattering cross section, Σ_s
BETA	Delayed neutron fraction, β
XL	Decay constant for the delayed neutron precursor, λ
W	Frequency
AX	X-dimension
BY	Y-dimension
CZ	Z-dimension
DEL	Large divisions in x and y directions
IB	Number of subdivisions in DEL
IO	Analytical solutions's Summation limit
XZ	Source location in x-direction

YZ	Source location in y-direction
ZZ	Source location in z-direction
SVALUE	Source magnitude in neutrons/second
XYZ	Specifying locations to be examined
	= z for IOPT1 = 1
	= Y and Z for IOPT = 2

B. Program Listing

```
C THIS PROGRAM CALCULATES THE ANALYTICAL SOLUTION OF THE
C FREQUENCY DEPENDENT NEUTRON DIFFUSION EQUATION USING
C THE TRIPLE SINE SUMMATION, THE TWO EXPONENTIAL TERMS,
C AND THE EIGHT EXPONENTIAL TERMS SOLUTION FORMS.
C SINCE THE SOLUTION IS FOR A THREE DIMENSIONAL
C MODLE, THE Z SURFACE MUST BE SPECIFIED AND THE X-Y
C SOLUTION WILL BE CALCULATED. THE SOLUTION CAN ALSO
C BE CALCULATED ALONG  X DIMENSION PROVIDED THAT THE
C Y AND Z VALUES ARE SPECIFIED.
      COMPLEX G1,G2,G4,GB,GC,GD,GE,GF,F1,F2,SUM1,SUM2,PD,P1
      COMPLEX P2,DUM1,DUM2,DUM3,DM1,DM2,R1,R2,R3,R4,R5,R6,XJJ
      COMPLEX B1,B2,B21,B22,B1J,B2J,PA1,PA2,PB1,PB2,EP1,EP2
      COMPLEX EM1,EM2,SUMF,SUMT,SUMP(2,8)

      COMMON AX,BY,CZ,PI,D(2),IB,DEL(6),IOPT1,XZ,YZ,ZZ
      COMMON AP,BP,CP,X,Y,Z,GA,IO,XP,XM,YP,YM,ZP,ZM,AX2
      COMMON BY2,CZ2,SVALUE,IOPT2
      DIMENSION FR(25,25),FI(25,25),TR(25,25),TI(25,25)
      DIMENSION XX(26),SIG(2),SIGF(2),SIGS(2,2),V(2),XYZ(2)
      DIMENSION RP(8)

      OPEN(11,STATUS='OLD',FILE='INPUT.DAT')

      READ (11,*) NOG,IOPT1,IOP2
      DO I = 1,NOG
      READ (11,*) D(I),SIG(I),SIGF(I),V(I)
      ENDDO
      READ (11,*) ((SIGS(I,J),J=1,NOG),I=1,NOG)
      READ (11,*) BETA,XL,W
      READ (11,*) AX,BX,CX
      READ (11,*) DEL
      READ (11,*) IO,IB
      READ (11,*) XZ,YZ,ZZ,SVALUE
      READ (11,*) (XYZ(I),I=1,IOPT1)

      Z = XYZ(IOPT1)
      IF (IOPT1.GT.1) Y = XYZ(IOPT1-1)

      DM1 = CMPLX(XL,W)
      Z1 = -SIG(1)-SIGS(2,1)+SIGF(1)*(1.0-BETA)
      Z2 = -W/V(1)
      DM2 = CMPLX(Z1,Z2)
      G1 = DM2+XL*BETA*SIGF(1)/DM1
      G2 = SIGF(2)*(1.0-BETA)+XL*BETA*SIGF(2)/DM1
      G3 = SIGS(2,1)
      G4 = CMPLX(-SIG(2),-W/V(2))
```

```
      GA = -D(1)*D(2)
      GB = G4*D(1)+G1*D(2)
      GC = G3*G2-G1*G4

      PI = 3.141592653
      AP = PI/AX
      BP = PI/BX
      CP = PI/CX

      GD = GA*2.0
      GE = GB*GB-4.0*GA*GC
      GF = CSQRT(GE)
C     R3 NEVER, R4 ALWAYS, R5 FOR W<1, R6 FOR W>1
      R1 = (-GB-GF)/GD
      R2 = (-GB+GF)/GD
      R4 = -CSQRT(R1)
      R5 = CSQRT(R2)
      R6 = -R5

      AX2 = AX*2.0
      BY2 = BY*2.0
      CZ2 = CZ*2.0

      B1 = R4
      B2 = R6
      IF (W.LT.1.0) B2 = R5
      B21 = B1*B1
      B22 = B2*B2

      XJJ = CMPLX(0.0,1.0)
      B1J = B1*XJJ
      B2J = B2*XJJ

      DUM1 = -D1*B21+DUM5
      DUM2 = 2.0*A*B21+DUM6
      DUM3 = A*B21*B21+DUM6*B21+DUM7
      PA1 = -DUM2/DUMH
      PB1 = (DUM2*DUM1+DUM3*D1)/(DUM1*DUM1)
      DUM1 = -D1*B22+DUM5
      DUM2 = 2.0*A*B22+DUM6
      DUM3 = A*B22*B22+DUM6*B22+DUM7
      PA2 = -DUM2/DUMH

      ZP = Z+ZZ
      ZM = Z-ZZ

      IF (IOPT1.GT.1) GO TO 60
      GO TO 70
60    YM = Y-YZ
      YP = Y+YZ

70    X = 0.0
```

```
      IG = 1
      DO 26 IDELX = 1,6
      DELX = DEL(IDELX)/IB
      IBB = IB
      IF (IDELX.EQ.6) IBB = IB+1
      DO 28 I = 1,IBB
      XP = X+XZ
      XM = X-XZ
      IH = 1
      IF (IOPT1.EQ.2) GO TO 30
      Y = 0.0
      DO 32 IDELY = 1,3
      DELY = DEL(IDELY)/IB
      IBBY = IB
      IF (IDELY.EQ.3) IBBY = IB+1
      DO 34 J = 1,IBBY
      YP = Y+YZ
      YM = Y-YZ
30    CONTINUE
      IF (IOPT2.NE.0)GO TO 80
      CALL SINES(GA,GB,GC,G1,G2,SUMF,SUMT)
      GO TO 90
80    CALL EXPON(GA,GB,GC,G1,G2,G3,G4,SUMF,SUMT)
90    CONTINUE
      FR(IG,IH) = REAL(SUMF)
      FI(IG,IH) = AIMAG(SUMF)
      TR(IG,IH) = REAL(SUMT)
      TI(IG,IH) = AIMAG(SUMT)
      IF(IOPT1.EQ.2) GO TO 32
      IH = IH+1
      Y = Y+DELY
34    CONTINUE
32    CONTINUE
      XX(IG) = X
      IG = IG+1
      X = X+DELX
28    CONTINUE
26    CONTINUE
      IF(IOPT.EQ.2) GO TO 98
      WRITE(7,56)
      WRITE(8,56)
      WRITE(9,56)
      WRITE(10,56)
```

```
 56   FORMAT('  25 25 1 1')
      WRITE(7,*)(XX(I),I = 1,25),(XX(I),I = 1,25)
      WRITE(8,*)(XX(I),I = 1,25),(XX(I),I = 1,25)
      WRITE(9,*)(XX(I),I = 1,25),(XX(I),I = 1,25)
      WRITE(10,*)(XX(I),I = 1,25),(XX(I),I = 1,25)
      WRITE(7,*)((FR(I,J),J = 1,25),I = 1,25)
      WRITE(8,*)((FI(I,J),J = 1,25),I = 1,25)
      WRITE(9,*)((TR(I,J),J = 1,25),I = 1,25)
      WRITE(10,*)((TI(I,J),J = 1,25),I = 1,25)

      STOP

 98   CONTINUE
      WRITE(11,*)(XX(I),I = 1,25)
      WRITE(7,*)(FR(I,1),I = 1,25)
      WRITE(8,*)(FI(I,1),I = 1,25)
      WRITE(9,*)(TR(I,1),I = 1,25)
      WRITE(10,*)(TI(I,1),I = 1,25)

      STOP
      END

      SUBROUTINE SINES(GA,GB,GC,G1,G2,SUMF,SUMT)
      COMPLEX G1,G2,G4,GB,GC,GD,GE,GF,F1,F2,SUM1,SUM2,PD,P1
      COMPLEX P2,DUM1,DUM2,DUM3,DM1,DM2,R1,R2,R3,R4,R5,R6,XJJ
      COMPLEX B1,B2,B21,B22,B1J,B2J,PA1,PA2,PB1,PB2,EP1,EP2
      COMPLEX EM1,EM2,SUMF,SUMT,SUMP(2,8)
      COMMON AX,BY,CZ,PI,D(2),IB,DEL(6),IOPT1,XZ,YZ,ZZ
      COMMON Y,Z
      DIMENSION FR(25,25),FI(25,25),TR(25,25),TI(25,25)
      DIMENSION XX(26),SIG(2),SIGF(2),SIGS(2,2),V(2),XYZ(2)
      DIMENSION RP(8)
C USING THE TRIPLE SINE SUMMATION FORMULATION FOR IOPT2 = 0

      SUM1=CMPLX(0.0,0.0)
      SUM2=CMPLX(0.0,0.0)
      DO 24 M = 1,IO
      BPM = M*BP
      YSIN = SIN(BPM*YZ)*SIN(BPM*Y)*XSIN
      BSY = BPM*BPM+BSX

      DO 24 N=1,IO
      CPN = N*CP
      ZSIN = SIN(CPN*ZZ)*SIN(CPN*Z)*YSIN
      BSZ = CPN*CPN+BSY
      BSZ2 = BSZ*BSZ

      PD = GA*BSZ2+GB*BSZ+GC
      P1 = PD/G2
      P2 = PD/(D(1)*BSZ-G1)

      SUM1 = SUM1+ZSIN/P1
      SUM2 = SUM2+ZSIN/P2
```

```
24   CONTINUE
     SUMF = 8.0E-6*SVALUE*SUM1
     SUMT = 8.0E-6*SVALUE*SUM2

     RETURN
     END

C USING THE EXPONENTIAL FORMULATIONS FOR IOPT2 = 2 OR 8
     SUBROUTINE EXPON(GA,GB,GC,G1,G2,G3,G4,SUMF,SUMT)
     COMPLEX G1,G2,G4,GB,GC,GD,GE,GF,F1,F2,SUM1,SUM2,PD,P1
     COMPLEX P2,DUM1,DUM2,DUM3,DM1,DM2,R1,R2,R3,R4,R5,R6,XJJ
     COMPLEX B1,B2,B21,B22,B1J,B2J,PA1,PA2,PB1,PB2,EP1,EP2
     COMPLEX EM1,EM2,SUMF,SUMT,SUMP(2,8)
     COMMON AX,BY,CZ,PI,D(2),IB,DEL(6),IOPT1,XZ,YZ,ZZ
     COMMON IO,AP,BP,CP,X,Y,Z,SVALUE,IOPT2
     DIMENSION FR(25,25),FI(25,25),TR(25,25),TI(25,25)
     DIMENSION XX(26),SIG(2),SIGF(2),SIGS(2,2),V(2),XYZ(2)
     DIMENSION RP(8)

     SUM1=CMPLX(0.0,0.0)
     SUM2=CMPLX(0.0,0.0)

     DO 38 IL = -IO,IO
     XOP = XP-IL*AX2
     XOM = XM-IL*AX2
     XPS = XOP*XOP
     XMS = XOM*XOM

     DO 38 IM = -IO,IO
     YOP = YP-IM*BY2
     YOM = YM-IM*BY2
     YPS = YOP*YOP
     YMS = YOM*YOM

     DO 38 IN = -IO,IO
     ZOP = ZP-IN*CZ2
     ZOM = ZM-IN*CZ2
     ZPS = ZOP*ZOP
     ZMS = ZOM*ZOM

     RP(1) = SQRT(XPS+YPS+ZPS)
     RP(2) = SQRT(XPS+YPS+ZMS)
     RP(3) = SQRT(XPS+YMS+ZMS)
     RP(4) = SQRT(XPS+YMS+ZPS)
     RP(5) = SQRT(XMS+YPS+ZMS)
     RP(6) = SQRT(XMS+YPS+ZPS)
     RP(7) = SQRT(XMS+YMS+ZPS)
     RP(8) = SQRT(XMS+YMS+ZMS)

     DO 40 IB = 1,8
     SUMP(1,IB) = CMPLX(0.0,0.0)
```

```
      SUMP(2,IB) = CMPLX(0.0,0.0)
40    CONTINUE

      NN = 1
      IF (IOPT2.EQ.2) NN = 7

      DO 42 IH = 1,8,NN
      EP1 = CEXP(B1J*RP(IH))
      EP2 = CEXP(B2J*RP(IH))
      SUMP(1,IH) = EP1/RP(IH)
      SUMP(2,IH) = EP2/RP(IH)
42    CONTINUE

      IF (IL.EQ.-IO) GO TO 44
      IF (IM.EQ.-IO) GO TO 44
      IF (IN.EQ.-IO) GO TO 44
      GO TO 46

44    SUMP(1,1) = CMPLX(0.0,0.0)
      SUMP(2,1) = CMPLX(0.0,0.0)
46    CONTINUE

      ISO = -1
      DO 48 IH = 1,8
      SUM1 = SUM1+ISO*SUMP(1,IH)
      SUM2 = SUM2+ISO*SUMP(2,IH)
      ISO = -ISO
48    CONTINUE

38    CONTINUE

      SUMF = (SUM1/PA1+SUM2/PA2)/12.56637061*SVALUE
      SUMT = (SUM1/PB1+SUM2/PB2)/12.56637061*SVALUE
      RETURN
      END
```

C. Sample Input File

```
2     1     2
1.5   0.01   0.00    3.6E6
0.4   0.08   0.14    2.2E5
0.0   0.0
0.02  0.0
0.0065   0.01   10.0
100.   100.   100.
30.0   15.0   05.0   05.0   15.0   30.0
15   4
50.0   50.0   50.0   48.0
16.0
```